IEEE Access
Multidisciplinary | Rapid Review | Open Access Journal

Received December 19, 2020, accepted December 29, 2020, date of publication January 4, 2021, date of current version January 13, 2021.

Digital Object Identifier 10.1109/ACCESS.2020.3049049

A Novel Hybridized Fuzzy PI-LADRC Based Improved Frequency Regulation for Restructured Power System Integrating Renewable Energy and Electric Vehicles

PRATEEK SHARMA, ABHISHEK MISHRA, ABHISHEK SAXENA, (Graduate Student Member, IEEE), AND RAVI SHANKAR

Department of Electrical Engineering, National Institute of Technology Patna, Patna 800005, India

Corresponding author: Ravi Shankar (ravi@nitp.ac.in)

ABSTRACT In this article, an Improved Frequency Regulation (IFR) for an interconnected hybrid power system under a deregulated scenario is proposed. The analyzed test system comprises of a thermal power system, biogas plant, and Distributed Generation (DG). The impact of the integration of Renewable Energy Sources (RES) has been examined by considering DG system with solar and wind power generation. In order to make the system more realistic, appropriate non-linearities are incorporated into the thermal and biogas system. Electric Vehicle (EV) is also employed to take care of some portion of uncontracted demand. A maiden hybridized fuzzy-Proportional Integral (FPI)-Linear Active Disturbance Rejection Control (LADRC) is proposed and successfully implemented for IFR. Also, a new Quasi-Opposition-based Artificial Electric Field Algorithm (QO-AEFA) is proposed to acquire the optimal controller gain parameters of the tested system. A pertinent performance analysis is also examined for other employed algorithm in this study, to figure out the eminence of the proposed control algorithm. A comprehensive examination and comparison of the proposed controller with other controllers shows its effectiveness for the proposed test system. In order to ensure the reliability of the proposed controller, sensitivity analysis is also carried out for system parameters that reveal its robust nature. Further, case studies for random load variations and comparison with the works in previous literature also manifest the puissance of the current research work. Moreover, the improved results under random weather conditions illustrate the effectiveness of the proposed IFR under deregulation.

INDEX TERMS Fuzzy-proportional integral (FPI), improved frequency regulation (IFR), linear active disturbance rejection control (LADRC), quasi-opposition based artificial electric field algorithm (QO-AEFA).

I. INTRODUCTION

Nowadays, the power system is mostly influenced by vertically integrated utilities (VIUs). The utilities possess their own generation, transmission, and distribution systems. They deliver power to the consumers according to Automatic Generation Control (AGC) norms. VIUs are connected with one another at the transmission voltage level [1]. AGC proved to be successful in VIUs, and it led to the evolution of a new restructured (deregulated) power system preserving the essential concepts of AGC. In the deregulated system, a price-based operation, as decided by the market structure, is adopted under the supervision of AGC.

Market policies, economic profits, and improved quality services to the consumers constitute the deregulation. Under a deregulated system, generation companies (GENCOs), distribution companies (DISCOs), and transmission companies (TRANSCOs), along with independent service operators, act independently and therefore are modeled separately. DISCOs have contracts with the GENCOs to supply the power, and this contractual relationship is reflected in the DISCO participation matrix [2], [3]. In this new structure, AGC is supposed to be more responsible in order to suppress the effects of deviation in the contractual demand to sustain quality services [4].

The associate editor coordinating the review of this manuscript and approving it for publication was Siqi Bu.

The deregulated power system has been studied by the researchers considerably and notable discussions have been carried out regarding the AGC of the interconnected power system (viz. VIUs). References [4], [5] have widely explained deregulation in the power system. The transition from a conventional paradigm (VIUs) to a new paradigm (horizontally integrated industry) is unveiled in [4], [6] along with various deregulation cases in the AGC system and its control technique.

The recent works on deregulation reveal that many optimization techniques have been adopted to aid the AGC performance in a deregulated environment. P.K. Hota *et al*. have suggested differential evolution for AGC under a deregulated environment in [7] to tune the parameters of PID controllers, where Generation Rate Constraint (GRC) is considered but Governor Dead Band (GDB) and Boiler Dynamics (BD) are omitted. Reference [2] presents a distributed model predictive control scheme for AGC of three areas interconnected system taking into account GRC and load reference point. GDB and BD are not considered here also. An investigation into the deregulated AGC domain employing fractional order proportional integral derivative (FO-PID) controller is presented in [8]. An application of a salp swarm differential evolution algorithm is studied in [9] in a deregulated scenario considering physical constraints and two degrees of freedom-tilt integral derivative (2DOF-TID) controller. Moreover, the 3DOF-PID controller is employed in [10] for frequency regulation (FR) of a nonlinear power system. Pertaining to controllers, several significant controllers have been introduced over the past few decades. Apart from conventional controllers[7], some other centralized controllers like fuzzy logic controllers (FLC), fractional-order controllers, model predictive controllers, etc have also been observed in FR. FLC, when utilized along with conventional controllers like proportional-integral (PI) and proportional integral derivative (PID) promptly improves the dynamic performance of the power system. They also deal with the discrepancies in system parameters. Particle swarm optimization- pattern search (PSO-PS) optimized fuzzy PI controller is introduced in[11]. Reference [12] reports a fuzzy adaptive model predictive control for load frequency control (LFC) of an isolated microgrid. Hybrid fuzzy logic intelligent PID controller for multiple area power network considering the physical constraints is visualized in [13]. Likewise, we see that the fractional calculus concept lays down the idea of fractional order (FO) controller in which the order of 's' is tuned to any real value [8]. Reference [14] realizes adaptive fractional-order fuzzy optimized by teaching learning-based optimization (TLBO) for power systems consisting of renewable sources reheat, GRC, and BD but GDB is omitted. The implication of fuzzy fractional order proportional integral-fractional order proportional derivative (FOPI-FOPD) controller is significantly observed in [15] to fairly meet the challenges of a multiarea electric power system. Moreover, [16] addresses the sliding mode control along with generalized estimated state observer (GESO) to regulate the frequency of two area power system network by accurately estimating the actual states of the system. Sahaj Saxena *et al.* have investigated internal model control for AGC of a single and multiple area system in the presence of uncertainty [17]. LADRC is proposed for the frequency regulation of microgrid in [18].

The power system has seen several developments like the integration of renewable sources, distributed generation, electric vehicles, artificial intelligence, etc. Distributed generation (DG) is a small energy source installed near the load point. It may consist of renewable/non-renewable energy sources like wind energy systems, photovoltaic systems, diesel systems, fuel cells, ultra-capacitors, etc. [9], [10]. DG helps to supply the power to the remote areas where transmission of power via the grid is not economical. However, DG presents some challenges to the power system therefore its operation needs to be supervised carefully. Assessment of frequency regulation is carried out for the DG system in [19], which employs the FOPID controller. Meanwhile, an analytical approach for restructured power systems integrating DG unit with combined application of redox flow battery and DC link for better system performance is elegantly presented in [20]. A modern power system is heading towards utilizing renewable energy sources to the maximum extent as they are pollution-free, noise-free, and eco-friendly. Reference [21] illustrates the application of renewable energy sources where wind turbine, solar generation, sea wave energy, energy storage system are taken in the marine power system. Fractional order fuzzy PD+I controller is chosen for frequency regulation.

Electric vehicles present a very good option for future electricity demand. They are pollution-free, and portable hence provides better service. Countries are aiming to increase the use of electric vehicles in the near future because of their ascendancy. Electric vehicle charges during off-peak load period i.e., from 10 pm to 8 am, and supplies during emergency or peak load period. Their dynamic response is good. One of the benefits of using EV is that in the competitive electricity market, when DISCOs sometimes demand uncontracted power, EVs prove beneficial due to their fast dynamic response [22]. However, their charging and discharging need to be appropriately regulated. The utilization of electric vehicles is discussed in [8], [22] in a deregulated power system. In [23] electric vehicles are connected along with other energy sources to supply power as a microgrid. A promising impact of electric vehicles for frequency regulation exhibits encouraging results in [24], and also improved system performances are observed for an interconnected multiarea power system.

Literature survey disclosed that several AGC techniques have been introduced in the power system, but they have certain drawbacks as some have considered non-linearity, while some have omitted. Also, the DG system is mostly taken as standalone and not connected to the grid. To fill this gap, an attempt is made in this work to provide the load frequency control in a deregulated interconnected power system containing reheat thermal power plant, DG, Biogas, and electric

vehicles. Fuzzy-PI aided LADRC is the proposed controller in the present work optimized by the QO-AEFA technique. Nonlinearity like governor dead-band (GDB), generation rate constraint (GRC), and boiler dynamics are considered to visualize a more realistic performance of the controller. The deregulated scenario is presented with EV and without EV to show the improvement in system performance because of EV. Sensitivity analysis is done to observe controller performance when system parameters are perturbed.

From the above discussions, the eminent highlights of the paper are as follows:

1) This work demonstrates an Improved Frequency Regulation (IFR) integrating distributed generation (DG) units and conventional power sources.
2) Electric vehicles are utilized to accomplish some portion of the uncontracted power demand of the analysed system in a deregulated environment.
3) A novel hybridized Fuzzy-Proportional Integral (FPI)-Linear Active Disturbance Rejection Control LADRC) technique is tested and proposed for IFR. Also, the supremacy and feasibility of the proposed controller are validated over other distinct controllers.
4) A new Quasi-Opposition based Artificial Electric Field Algorithm (QOAEFA) is proposed to acquire the various controller gain parameters of the test system. Additionally, the dynamic performance of the proposed algorithm is verified with some other algorithms in the literature.
5) In order to assure the robustness of the proposed controller, sensitivity analysis with wide variations in system parameters and a study for random weather conditions is presented. Also, a case study for random load variation followed by a comparison with previously published work of literature on the same platform is performed.

II. INVESTIGATED MULTI-AREA SYSTEM UNDER DEREGULATION

A. DEREGULATED AGC STUDY

A deregulated power system comprises three types of transactions namely pool-based (unilateral), bilateral, and contract violation, which function according to the AGC norms. The purpose of AGC is to ensure that the system frequency remains within a specified range, tie-line power flow is close to its scheduled value, and the economic operation of the generation units has prevailed. In a unilateral transaction, DISCOs of a particular area can buy power at the competitive price from the GENCO of the same control area [25], [26]. In a bilateral transaction, DISCOs are free to purchase power from the GENCO of any area through tie-lines. GENCOs report the contractual agreement with DISCOs to Independent System Operator (ISO) and continuously supervise that the demanded power is supplied to the DISCOs until it is below the contracted value. Also, the DISCOs monitor their loads to ensure that they follow the agreements with GENCOs [27]. Talking about the contract violation, it is a special case in the above two transactions wherein DISCOs violate the contractual agreement and demand extra power from the GENCOs. Moreover, this extra power is supplied by the GENCO of the same area in which DISCO infringes the contract.

The manner in which DISCOs contract the power from GENCOs is represented by the DISCO participation matrix (DPM). Each entry of the DPM is called the contract participation factor (cpf). cpf demonstrates the fraction of total power contracted by a particular DISCO from the respective GENCO. The cpf is chosen in such a way that the sum of all the cpfs in a particular column is equal to 1.

$$\text{i.e.} \quad \sum_{i=1}^{NGENCO} cpf_{ij} = 1; \quad \text{for } j = 1, 2 \ldots\ldots N\ DISCO \tag{1}$$

where NGENCO is the total no. of GENCOs and NDISCO is the total no. of DISCOs present in the system considered. Moreover, the contracted power by i^{th} GENCO with the DISCOs can be visualized by the following expression.

$$\Delta P_{gci} = \sum_{j=1}^{NDISCO} cpf_{ij} \Delta P_{Lj}; \quad \text{for } i = 1, 2 \ldots\ldots NGENCO \tag{2}$$

where ΔP_{gci} represent the power contracted by i^{th} GENCO and ΔP_{Lj} signifies the total load demanded by j^{th} DISCO. Furthermore, the no. of rows of the DPM is equal to the no. of GENCOs and the no. of columns is equal to the no. of DISCOs. In this work, two area power system is considered with three GENCOs and two DISCOs in each area. Thus, the DPM for the concerned system can be written as:

$$DPM = \begin{bmatrix} cpf_{11} & cpf_{12} & cpf_{13} & cpf_{14} \\ cpf_{21} & cpf_{22} & cpf_{23} & cpf_{24} \\ cpf_{31} & cpf_{32} & cpf_{33} & cpf_{34} \\ cpf_{41} & cpf_{42} & cpf_{43} & cpf_{44} \\ cpf_{51} & cpf_{52} & cpf_{53} & cpf_{54} \\ cpf_{61} & cpf_{62} & cpf_{63} & cpf_{64} \end{bmatrix} \tag{3}$$

Additionally, if there is more than one GENCO, they share the ACE (area control error) according to their ACE participation factor (apf). ACE is distributed among the GENCOs according to apf, which is decided by the profile of a GENCO, its contribution, bid price, and size in frequency regulation. Total load is shown by the local load demand in each area which is the sum of the load contracted by DISCOs in a particular area. GENCOs and DISCOs share the power relationship in three ways: pool-based, bilateral, and contract violation. The deviation of the actual tie-line power flow from the scheduled one is called the tie line error and is given as:

$$\Delta P_{tieerror} = \Delta P_{tie\_actual} - \Delta P_{tie\_scheduled} \tag{4}$$

$$\begin{aligned} \Delta P_{tie\_scheduled} &= P_{exp} - P_{imp} \\ &= [\text{load demand by DISCOs of Area} \\ &\quad -2\text{from the GENCOs of Area} - 1] \\ &\quad -[\text{load demand by DISCOs of Area} \\ &\quad -1\text{from the GENCOs of Area-2}] \end{aligned} \tag{5}$$

B. DESIGNING ASPECTS OF A DEREGULATED POWER SYSTEM MODEL

The efficacy of QO-AEFA and the proposed controller is justified on a test system which is two areas interconnected deregulated power system. A simplified layout of the test system is presented in Fig. 1. The controller output is shared by the GENCOs according to their ACE participation factor (apf). Considered apf for GENCO-1 to GENCO-6 are $apf_1 = 0.5$, $apf_2 = 0.3$, $apf_3 = 0.2$, $apf_4 = 0.5$, $apf_5 = 0.3$, and $apf_6 = 0.2$ respectively. The generating units are modeled as follows:

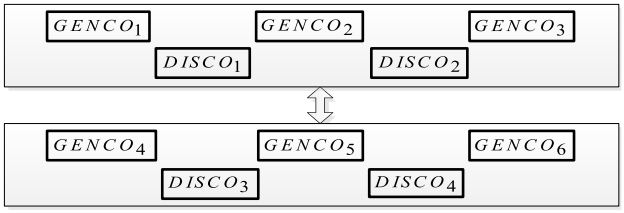

FIGURE 1. The layout of two area deregulated test power system.

C. THERMAL POWER PLANT

This consists of a governor and reheat turbine. The non-linearities like GDB, BD, and GRC are considered. GRC is 10% per minute i.e. 0.0017 pu/second. The transfer function model of the thermal power plant can be realized in Fig. 2 (a) and boiler dynamics by Fig. 2 (b).

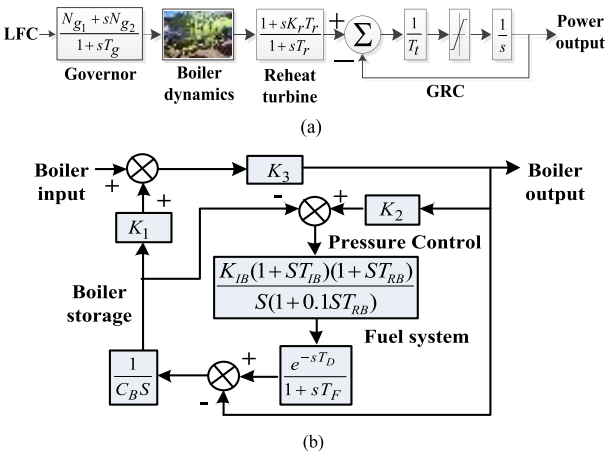

FIGURE 2. (a) Thermal power plant with non-linearity. (b) Boiler dynamics.

Where T_g and T_t represent time constant of steam governor and turbine, K_r and T_r represent steam turbine reheat coefficient and time constant, N_{g1} and N_{g2} are dead band coefficients, K_1, K_2, and K_3 are system parameters, K_{IB}, T_{IB}, and T_{RB} are the boiler integral gain, proportional-integral gain ratio, and lead-lag compensator time constant, T_D and T_F are the fuel firing delay and fuel time constant respectively, C_B signifies boiler's storage time constant.

D. SOLAR PHOTOVOLTAIC (SPV)

The energy coming from the sun is in two forms: light energy and heat energy. SPV utilizes the light energy of the sun and converts it into electrical energy. The photovoltaic system produces a direct current which is converted to ac by using an electronic convertor. The mechanism consists of a solar module and other electrical accessories. The SPVs can be connected to the grid or it can serve as a standalone system. The first-order transfer function of the SPV can be realized as:

$$G_{SPV} = \frac{K_{SPV}}{1 + sT_{SPV}} \tag{6}$$

where K_{SPV} and T_{SPV} are the gain & time constant of a solar photovoltaic system.

E. WIND TURBINE SYSTEM (WTS)

This mechanism converts the kinetic energy of the wind into electricity. The geographical areas which are bestowed with high wind velocity may act as a suitable location for the installation of WTS. In WTS there is a wind turbine, generator (induction or synchronous), gear arrangement, and power electronic devices. The first-order transfer function of the WTS can be given as:

$$G_{WTS} = \frac{K_{WTS}}{1 + sT_{WTS}} \tag{7}$$

where K_{WTS} and T_{WTS} are the gain & time constant of a wind turbine system.

F. DIESEL ENGINE GENERATOR (DEG)

The operation of DEG is based on the principle of the Carnot cycle. It has two parts: a diesel engine and an alternator to produce electricity. Inside the cylindrical chamber, the air is compressed at high pressure. Diesel is used as fuel for combustion inside the cylinder. The transfer function for DEG is:

$$G_{DEG} = \frac{K_{DEG}}{1 + sT_{DEG}} \tag{8}$$

where K_{DEG} and T_{DEG} are the gain & time constant of a diesel engine.

G. BATTERY ENERGY STORAGE SYSTEM (BESS)

BESS stores the chemical energy and supplies electrical energy. Its dynamic response is faster and it supports the mitigation of fluctuation in the system. The transfer function of BESS can be realized as:

$$G_{BESS} = \frac{K_{BESS}}{1 + sT_{BESS}} \tag{9}$$

where K_{BESS} and T_{BESS} are the gain & time constant of a battery energy storage system.

H. FUEL CELL (FC)

Fuel cell stores chemical energy of a fuel (hydrogen) and converts it directly into electrical energy. Fuel cells have many advantages like they are less pollutant and have high

efficiency etc. The linearized transfer function of FC can be realized as follows:

$$G_{FC} = \frac{K_{FC}}{1 + sT_{FC}} \tag{10}$$

where K_{FC} and T_{FC} are the gain & time constant of a fuel cell.

I. AQUA ELECTROLYZER (AE)

This is used to produce hydrogen to be used as fuel for a fuel cell. AE utilizes part of the wind and solar power to produce hydrogen. The transfer function of AE is:

$$G_{AE} = \frac{K_{AE}}{1 + sT_{AE}} \tag{11}$$

where K_{AE} and T_{AE} are the gain & time constant of an aqua electrolyzer.

J. FLYWHEEL ENERGY STORAGE SYSTEM

FESS is an electromechanical battery. It has a rotating flywheel to store mechanical energy (kinetic energy) which is converted to electrical energy when required later on. The expression of stored kinetic energy is given as:

$$E = \frac{1}{2} I\omega^2 \tag{12}$$

where I represent the moment of inertia and ω is the rotational velocity. FESS has many advantages like it does not use any chemical, is pollution-free, durable, etc., the transfer function can be realized as:

$$G_{FESS} = \frac{K_{FESS}}{1 + sT_{FESS}} \tag{13}$$

K_{FESS} and T_{FESS} are the gain & time constant of a flywheel energy storage system.

K. COMPLETE MODEL OF DG UNIT

The various discussed generating sources of DG [9] are connected in a fashion that is shown in Fig. 3. It can be seen that part of the output of WTS and SPV is given to AE to produce hydrogen which is utilized by the fuel cell as a fuel. A variable load perturbation is given to WTS and SPV. LFC signal is fed to the DEG, BESS, and FESS.

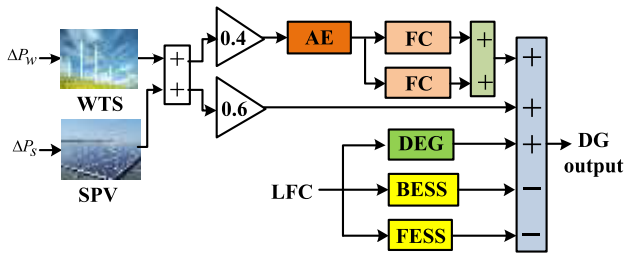

FIGURE 3. Interconnection of distributed generation.

L. BIOGAS TURBINE GENERATOR (BGTG)

The biodegradable wastes and animal droppings can be used for producing biogas. Biogas is a non-conventional fuel and can be used in biogas turbine generators to produce electricity. BGTG comprises of the inlet valve, governor, combustor, and turbine. GRC is considered for the turbine and its value is 20% per minute, i.e., 0.0033 pu/second. BGTG can be visualized by Fig. 4 as a linearized transfer function:

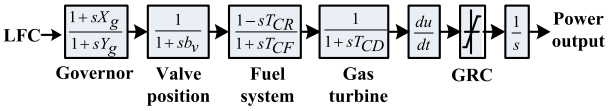

FIGURE 4. Biogas turbine generator model with open-loop GRC.

Where X_g and Y_g represent lead and lag time constant of biogas governor unit, b_v and T_{CD} are the valve actuator and discharge delay, T_{CR} and T_{CF} are the combustion reaction delay & bio-gas delay respectively.

M. MODELLING OF ELECTRIC VEHICLE

Electric vehicles present a very good option for future electricity demand. They are pollution-free and portable hence provide better service. Countries are aiming to increase the use of electric vehicles in near future because of their ascendancy. Electric vehicle charges during off-peak load period i.e., from 10 pm to 8 am, and supplies during emergency or peak load period. Their dynamic response is good. One of the benefits of using EV is in the competitive electricity market, where DISCOs may sometimes demand uncontracted power. Because of their fast dynamic response, EVs prove beneficial in such situations and take care of uncontracted power [22]. However, their charging and discharging need to be properly regulated.

The EV design is taken from [8] and [22]. Decentralized or droop control of the EV fleet is adopted. EV contributes to the frequency regulation according to area control error (ACE). The conventional model of EV is shown in Fig. 5. Dead-band is provided to restrict the EV operation under slight fluctuation. The upper and lower limit of dead-band is Δf_{ul} and Δf_{ll} (+10 mHz and -10 mHz) respectively. R_{EV} is the droop coefficient, $\Delta P^{\max}$ and $\Delta P^{\min}$ denote the maximum and minimum power reserve of EV fleet respectively, and are calculated as given in (14) and (15).

$$\Delta P^{\max} = +\left[\frac{1}{N_{EV}}\right]\Delta P_{EV} \tag{14}$$

$$\Delta P^{\min} = -\left[\frac{1}{N_{EV}}\right]\Delta P_{EV} \tag{15}$$

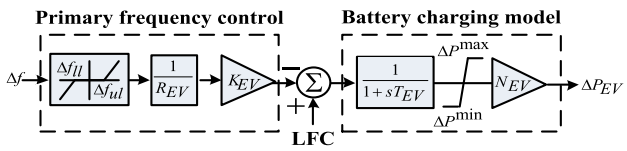

FIGURE 5. Conventional model of electric vehicle.

where K_{EV} is EV gain, T_{EV} represents the time constant of the battery, and N_{EV} reflects the number of EV'S. EV gain supervises the participation of EV in frequency regulation. The value K_{EV} is decided by the SOC (state of charge) of the EV battery as illustrated in Fig. 6 (a) where idle mode or discharge is shown. From Fig. 6 (a) it can be inferred that when SOC is below SOC_1, EV does not participate in frequency regulation. From SOC_1 to SOC_2 it participates partially whereas from SOC_2 onwards EV fully participates in FR [28]. Fig. 6 (b) shows the relationship between the average value of EV'S gain K_{AV} and the average value of the state of charge SOC_{AV}.

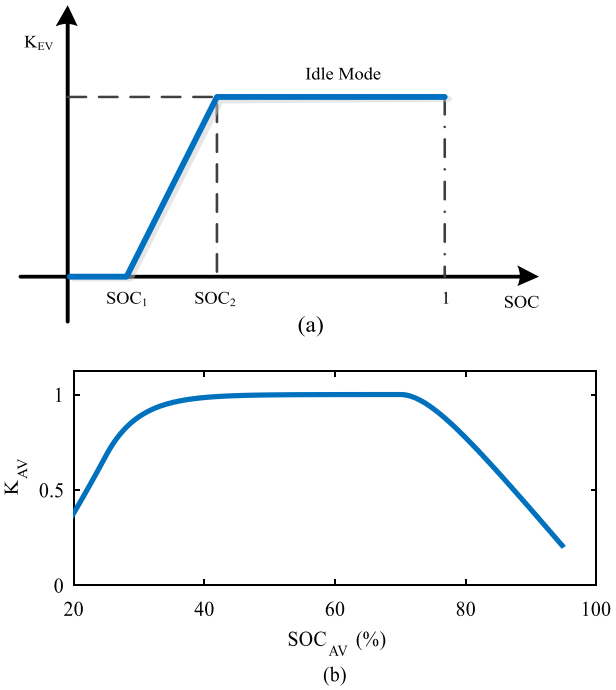

FIGURE 6. Characteristic of (a) KEV versus SOC in idle mode condition. (b) K_{AV} versus SOC_{AV}.

The power exchange between EV and grid is controlled by a battery charger. The power output of EV according to ACE is given as [24]:

$$\Delta P_{EV} = \begin{cases} K_{EV} \cdot ACE, & |K_{EV} ACE| \leq \Delta P^{\max} \\ \Delta P^{\max}, & |K_{EV} \cdot ACE| > \Delta P^{\max} \\ \Delta P^{\min}, & |K_{EV} \cdot ACE| < \Delta P^{\min} \end{cases} \quad (16)$$

when the power output of EV lies outside the limit, EV does not participate in the frequency regulation. Having injected power to the grid, the SOC of EV battery changes and the new SOC can be calculated by:

$$SOC_{new} = SOC_{old} - \left(\frac{\Delta E}{E_{rated}} \right) \quad (17)$$

where SOC_{new} is the new value of SOC after injecting energy ΔE , SOC_{old} is the rest SOC before the injection of energy, and E_{rated} is the rated EV capacity. The injected energy ΔE can be estimated as:

$$\Delta E = P_{inj} . \Delta t \quad (18)$$

where P_{inj} is the injected power in Δt time. EV participates in the frequency regulation by charging or discharging power. While using discharging power the gain K_{EV} increases by increasing SOC. On the other hand, when it uses charging power, the gain K_{EV} decreases with an increase in SOC. The zero value of K_{EV} indicates that the SOC of the EV battery is not adequate for EV to take part in frequency regulation. Numerical values for the simulation study are: $K_{EV} = 1$, $R_{EV} = 2.4$Hz/puMW $T_{EV} = 1s$, $N_{EV} = 10000$.

The complete design of the proposed AGC model in a deregulated environment is portrayed in Fig. 7 which consists of two identical areas with 2000 MW capacity each and having three GENCOs and two DISCOs.

In Fig. 7, subscript i represent area-i, Δf_i is the frequency deviation in area-i, ΔP_{tie} is the tie-line power deviation in areas (pu MW), T_{ij} is the synchronizing coefficient with area-j, K_{Pi} and T_{Pi} are the gain and time constant of a power system, B_i and R_i are the frequency bias coefficient and speed droop characteristic of area-i, δ_i denotes participation factor of AGC units in area-i.

III. DESIGN AND IMPLEMENTATION OF THE PROPOSED CONTROLLER

A. STRUCTURE OF PIDN CONTROLLER

PIDN controller is a PID controller with a filter. PID controller is composed of proportional, integral, and derivative controller. The proportional controller improves system dynamic behavior by decreasing the rise time. The integral controller reduces the steady state error to zero but adds a pole to the system transfer function. The derivative controller adds zero to the transfer function and improves the stability of the system, it reduces the overshoot and improves the dynamic behavior. The complete diagram of the PIDN controller is reflected in Fig. 8. The overall transfer function of the PIDN controller is given as:

$$TF = K_{Pii} + K_{Iii} \left(\frac{1}{s} \right) + K_{Dii} \frac{N_i}{s + N_i} \quad (19)$$

B. STRUCTURE OF FUZZY PI CONTROLLER

Input to the fuzzy PI controller is ACE and its derivative. The output of the fuzzy-PI controller is added with that of LADRC and fed to the GENCOs according to their apf. There are mainly three functions associated with FLC: fuzzification, decision making, and defuzzification. In fuzzification, crisp input data is mapped into fuzzy data with the help of membership functions. FLC employs triangular membership function [30] for error, a derivative of the error and output, and has 7 fuzzy linguistic variables which are: LN(low negative), MN(medium negative), SN(small negative), Z(zero), SP(small positive), MP(medium positive) and LP(low positive). Mamdani interface engine is chosen for fuzzy action to

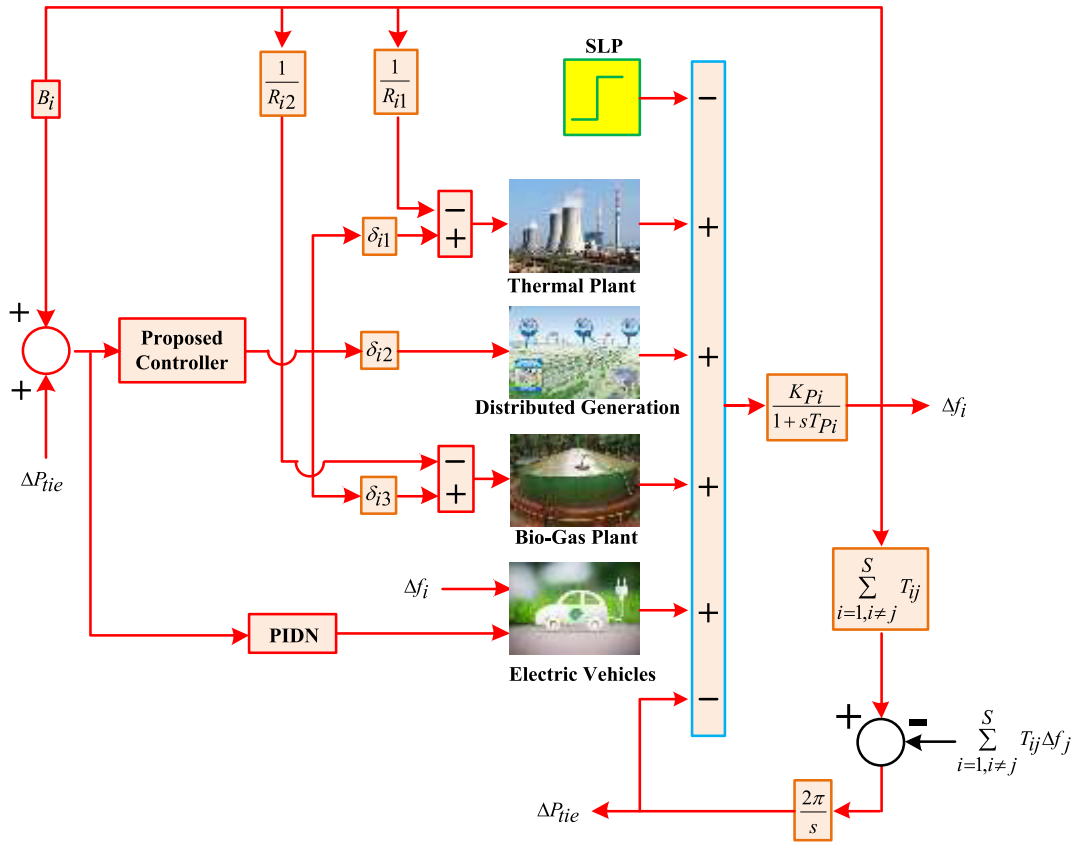

FIGURE 7. Complete model of two area deregulated test power system under investigation.

TABLE 1. Two-dimensional rule base for Fuzzy-PI controller.

ACE	$\dot{ACE}$						
	LN	MN	SN	Z	SP	MP	LP
LN	LP	LP	LP	MP	MP	SP	Z
MN	LP	MP	MP	MP	SP	Z	SN
SN	LP	MP	SP	SP	Z	SN	MN
Z	MP	MP	SP	Z	SN	MN	MN
SP	MP	SP	Z	SN	SN	MN	NL
MP	SP	Z	SN	MN	MN	MN	NL
LP	Z	SN	MN	MN	NL	NL	NL

make decisions based on a rule base. The two-dimensional rule base is taken from [30] and is given in Table 1. Now the output of the FLC is in the fuzzy form which is converted to crisp value. This is called defuzzification which is accomplished here by the centroid method. The membership function for ACE, its derivative, and output is the same and shown by Fig. 9. The fuzzy logic controller (FLC) is cascaded with the PI controller shown in Fig. 10 to form a fuzzy-PI controller [29]. The crisp output of the FLC is fed to the PI controller.

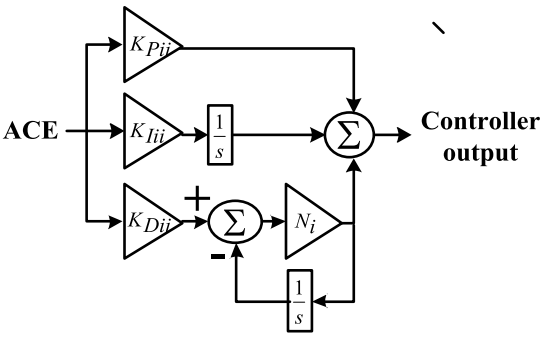

FIGURE 8. PIDN controller.

C. STRUCTURE OF LADRC CONTROLLER

In the current work, as the system is non-linear simple ADRC approach will present many parameters to be tuned. Therefore to simplify the effort, a linear ADRC of second order is accepted [31] here, which is explained below:

Consider a typical second-order system which is represented by –

$$\ddot{y} = bu + f\,(\dot{y}, y, u, d) \tag{20}$$

where 'b' is the process parameter, u is the control force, d is the external disturbance, and $f\,(\dot{y}, y, u, d)$ is a total disturbance. One advantage in LADRC is that the disturbance need

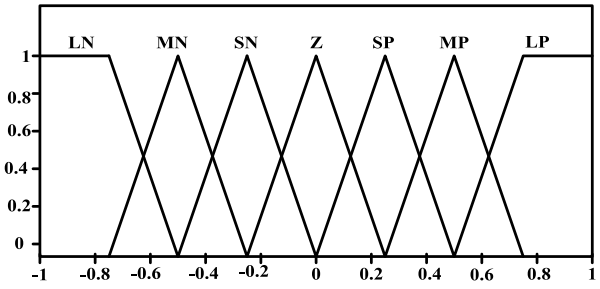

FIGURE 9. Membership function for input and output of FLC.

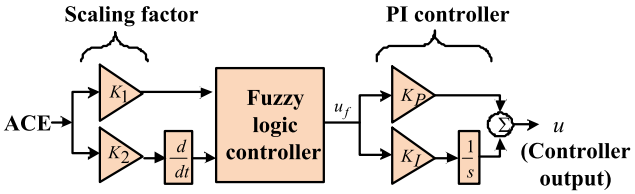

FIGURE 10. Fuzzy-PI controller.

not be modeled mathematically. Therefore where modeling of the system is not feasible there also the disturbance can be rejected. The state-space equation of the system represented by (20) can be written as:

$$\begin{cases} \dot{x}_1 = x_2 \\ \dot{x}_2 = b_0 u + x_3 \\ \dot{x}_3 = h \\ y = x_1 \end{cases} \tag{21}$$

where $x_1 = y, x_2 = \dot{y}, x_3 = f(\dot{y}, y, u, d)$, and $h = \dot{f}(\dot{y}, y, u, d)$. Here we see that for the disturbance, f an extended state is considered as x_3. Now the concept is to design an observer that estimates the state of the system. This information is used to design a control law that mitigates the error caused by disturbance thus rejecting the disturbance. The observer is designed as follows-

$$\begin{cases} \dot{z} = A_0 z + B_0 u + L_0 \left(y - \hat{y}\right) \\ \hat{y} = C_0 z \end{cases} \tag{22}$$

where $A_0 = \begin{bmatrix} 0 & 1 & 0 \\ 0 & 0 & 1 \\ 0 & 0 & 0 \end{bmatrix}, B_0 = \begin{bmatrix} 0 \\ b_0 \\ 0 \end{bmatrix}$ and $C_0 = \begin{bmatrix} 1 & 0 & 0 \end{bmatrix}$. $\hat{y}$ is the estimated value of y. b_0 is the estimated value of b and it can be tuned or calculated from the plant transfer function. $z = \begin{bmatrix} z_1 & z_2 & z_3 \end{bmatrix}^T$ is the estimated value of $x = \begin{bmatrix} x_1 & x_2 & x_3 \end{bmatrix}^T L_0 = \begin{bmatrix} \beta_1 & \beta_2 & \beta_3 \end{bmatrix}^T = \begin{bmatrix} 3\omega_o & 3\omega_o^2 & \omega_o^3 \end{bmatrix}^T$ is an observer gain vector and is obtained by the pole-placement method. ESO is written as:

$$\begin{cases} \dot{z}_1 = z_2 + \beta_1 (y - z_1) \\ \dot{z}_2 = z_3 + \beta_2 (y - z_1) + b_0 u \\ \dot{z}_3 = \beta_3 (y - z_1) \end{cases} \tag{23}$$

Here observer calculates the estimated value of x_3, i.e., total disturbance. Thereafter disturbance can be rejected by designing a suitable control law. The control law is as follows-

$$u = \frac{\left(-\hat{f} + u_0\right)}{b_0} \tag{24}$$

This reduces the original plant into a very simple form:

$$\ddot{y} = \left(f(\dot{y}, y, u, d) - \dot{f}\right) + u_0 \approx u_0 \tag{25}$$

Now one of the simple combinations for u_0 is simple PD controller as follows-

$$u_0 = k_p (r - z_1) - k_d z_2 - z_3 \tag{26}$$

k_p, k_d are the proportional and derivative controller gains, 'r' is the reference or set value which is generally the negative of ACE. The spatial diagram of the second-order LADRC model is shown in Fig. 11.

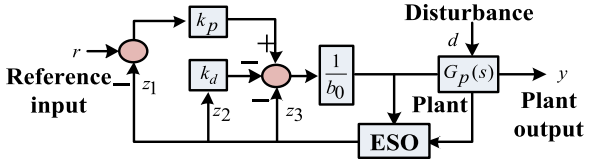

FIGURE 11. Second order LADRC.

As suggested by [31] controller and observer gains are a linear function of controller and observer bandwidth hence the name linear ADRC and can be represented as $k_p = \omega_c^2, k_d = 2\omega_c$ and $L_0 = \begin{bmatrix} \beta_1 & \beta_2 & \beta_3 \end{bmatrix}^T = \begin{bmatrix} 3\omega_o & 3\omega_o^2 & \omega_o^3 \end{bmatrix}^T$. Where k_p and k_d are controller gains, β_1, β_2 and β_3 are observer gains, ω_c is controller bandwidth and ω_o is observer bandwidth. Here we see that there are only two parameters ω_c and ω_o to be tuned. The estimated value of b i.e. b_0 can be calculated as follows-

Let the transfer function of the plant be

$$G_P(s) = \frac{b'_m s^m + b'_{m-1} s^{m-1} + \ldots\ldots\ldots b'_0}{a_n s^n + a_{n-1} s^{n-1} + \ldots\ldots\ldots a_0} \tag{27}$$

Then $b = \frac{b'_m}{a_n}$

The value of b_0 is taken as somewhat higher than b. It can also be tuned between specific ranges.

D. PROPOSED CONTROLLER

A maiden controller is proposed and successfully implemented for the proposed AGC mechanism. This proposed controller is a hybridization of Fuzzy PI and LADRC as portrayed in Fig. 12. The input of the controller has been taken as Area Control Error (ACE) and is given as:

$ACE = B_i \Delta f_i + \Delta P_{tie,error}$; where i represent the control area.

Based upon the error value controller generates its output which is fed to the GENCOs according to their apf. The desired task from the controller here is to supervise the AGC mechanism and ensure error minimization while improving the dynamic performance of the system.

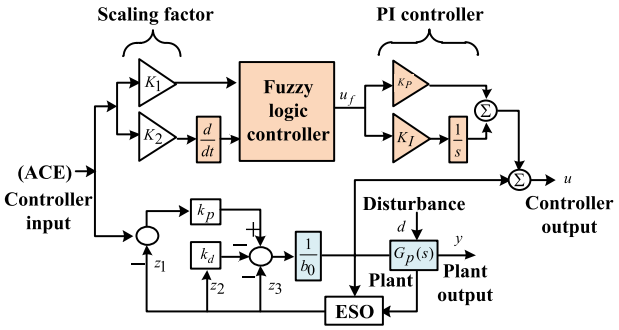

FIGURE 12. Novel hybridized Fuzzy PI-LADRC controller.

Let the output of the fuzzy logic controller is u_f then the output of fuzzy-PI controller can be expressed as:

$$u_1 = u_f K_P + \frac{u_f K_I}{s} \tag{28}$$

whereas the output of LADRC is given as:

$$u_2 = \frac{-\hat{f} + u_0}{b_0} \tag{29}$$

Now the output of the proposed controller can be written as:

$$u = u_1 + u_2$$
$$u = \left[u_f K_P + \frac{u_f K_I}{s}\right] + \left[\frac{-\hat{f} + u_0}{b_0}\right] \tag{30}$$

The proposed controller takes care of non-linearity in the system as well as known and unknown disturbances present in the system. The ascendency of the controller is justified by evaluating its performance in various situations. The analysis is presented in the simulation results and discussions section.

IV. AGC OBJECTIVE FUNCTION FORMULATION

In AGC, the objective function is generally the expression of error which is minimized using the metaheuristic optimization technique. Generally, there are four types of objective functions being used in literature. They are:

$$J_{\text{ITAE}} = \int_0^T \left\{(t * |\Delta f_1|) + (t * |\Delta f_2|) + \left(t * | \Delta P_{tie\_error} |\right)\right\} dt \tag{31}$$

$$J_{\text{ITSE}} = \int_0^T \left\{\left(t * \Delta f_1^2\right) + \left(t * \Delta f_2^2\right) + \left(t * \Delta P_{tie\_error}^2\right)\right\} dt \tag{32}$$

$$J_{\text{ISE}} = \int_0^T \left\{\Delta f_1^2 + \Delta f_2^2 + \Delta P_{tie\_error}^2\right\} dt \tag{33}$$

$$J_{\text{IAE}} = \int_0^T \left\{| \Delta f_1 + \Delta f_2 + \Delta P_{tie\_error} |\right\} dt \tag{34}$$

ITAE stands for Integral Time Absolute Error, ITSE stands for Integral Time Square Error, ISE stands for Integral Square Error and IAE stands for Integral Absolute Error. For different situations and systems, they show different behavior. Based on the type of action required, these objective functions are chosen for a particular system. IAE and ISE emphasize the initial value of error whereas ITAE and ITSE have a time-weighted function that emphasizes the error's final value. For the LFC problem, ITAE is more appropriate as it gives less settling time and overshoot. An analysis is done with all the error functions and ITAE is found to be better among all. The analysis is shown in the tabular form in Table 2 along with tuned parameter values in Table 3. Hence for further analysis in the paper, ITAE is chosen as the objective function owing to its better system dynamic responses. For the test system, ITAE offers the least maximum deviation in area-1 frequency, area-2 frequency, and tie-line power flow i.e., 0.0106 Hz, 0.0106 Hz, and 3.30E-04 puMW respectively. Also, the settling time for frequency deviation in area-1, frequency deviation in area-2, and tie-line power flow are 4.99 s, 4.49 s, and 10.78 s, respectively, which is firmly presented in Table 2. Also, from Fig. 13 we observed that the ITAE offers improved system dynamic performances in terms of maximum deviation and settling time for the investigated system. In the analysis, the power system model without deregulation is considered and local load disturbance is considered to be 0.01 pu.

TABLE 2. Analysis of system performance for different error function.

Error function	Δf_1		Δf_2		ΔP_{tie_error}	
	M.D (Hz)	S. T (s)	M. D (Hz)	S.T (s)	M.D (puMW)	S.T (s)
IAE	0.0014	12.37	8.15E-04	13.31	3.18E-04	36.36
ISE	0.0113	12.40	0.011	12.91	4.84E-04	24.56
ITSE	0.0113	12.40	0.011	12.91	4.84E-04	24.56
ITAE	**0.0106**	**4.99**	**0.0106**	**4.49**	**3.30E-04**	**10.78**

V. PROPOSED QUASI OPPOSITION-BASED ARTIFICIAL ELECTRIC FIELD ALGORITHM (QO-AEFA)

The controller parameters need to be tuned effectively so as to obtain better control. There are various optimization techniques available out there that help to tune the controller parameters to minimize the system errors. Some of the optimization techniques being Particle Swarm Optimization (PSO) [32], Teaching Learning Based Optimization (TLBO) [33], Grey Wolf Optimization (GWO) [34], Whale Optimization (WO) [35], etc. In the studied work, Quasi Opposition-based Artificial Electric Field Algorithm (QO-AEFA) is used which is a new technique and has never been used for LFC in the literature so far.

AEFA is a metaheuristic technique which is inspired by Coulomb's law of electrostatic force [36]. The law states that the electrostatic force of attraction or repulsion between two charged particles is directly proportional to the product of the magnitude of the charges and inversely proportional to the square of the distance between the charge centers. In this technique force of attraction is considered only. Charges represent the fitness of the population. They are spread

TABLE 3. Tuned parameter values for error function analysis.

Controller gains	IAE	ISE	ITSE	ITAE
ω_{c_1}	1.0258	1.417	1.3119	**0.9802**
ω_{c_2}	1.0524	1.0636	1.2348	**0.6942**
ω_{o_1}	4.3538	6.1546	5.8225	**5.5865**
ω_{o_2}	2.7834	3.7219	5.4604	**8.8472**
k_1	0.0092	0.5848	0.4571	**0.0671**
k_2	0.2482	0.8798	0.4561	**0.9745**
K_{P_1}	1.8228	0.8338	1.1897	**1.3814**
K_{I_1}	1.508	0.8598	1.0233	**1.8374**
k_3	0.2744	0.2952	0.485	**0.2048**
k_4	0.9433	0.4492	0.7605	**0.8262**
K_{P_2}	1.6951	1.2281	1.3499	**1.8888**
K_{I_2}	1.7635	0.9136	1.0035	**1.0814**
$K_{P_{11}}$	1.7988	1.393	1.1014	**1.8314**
$K_{I_{11}}$	0.2384	1.4708	0.4423	**1.7548**
$K_{D_{11}}$	0.73	0.7566	0.9413	**0.1591**
$K_{P_{22}}$	0.2704	0.6184	0.8728	**1.8401**
$K_{I_{22}}$	1.6707	0.7817	0.7493	**1.7348**
$K_{D_{22}}$	1.2729	0.7745	0.8527	**0.391**
N_1	54.9313	55.2926	48.0381	**87.2271**
N_2	54.7482	29.712	45.174	**75.6234**

randomly in the search space. Quasi opposition based learning is applied to the AEFA. This technique gives fast convergence of the optimizing process. A quasi opposite point is found to have more probability of being close to the optimal solution [37]. The first population of the particles is generated randomly followed by calculation of opposite number given as:

$$X_{oi} = a_i + b_i - X_i \tag{35}$$

where X_i is the position of an ith particle and X_{oi} is the opposite number corresponding to X_i. After that quasi-opposite number is calculated by using:

$$X_{qoi} = rand(C_i, X_{oi}) \tag{36}$$

where $C_i = \frac{a_i+b_i}{2}$

X_{qoi} is a random number between C_i and X_{oi}.

The force acts upon the charges causing them to move towards the equilibrium position. The force acting on a charge i from charge j at any time t is given by:

$$F_{ij}^d(t) = K(t)\frac{Q_i(t)^* Q_j(t)\left(P_j^d(t) - X_i^d(t)\right)}{R_{ij}(t) + \varepsilon} \tag{37}$$

where $K(t)$ is Coulomb's constant at any time t, $Q_i(t)$ and $Q_j(t)$ are charges of ith and a jth particle at any time t, ε is the small positive constant and $R_{ij}(t)$ is the Euclidian distance between two particles i and j which is expressed as:

$$R_{ij}(t) = \left\|X_i(t), X_j(t)\right\|_2 \tag{38}$$

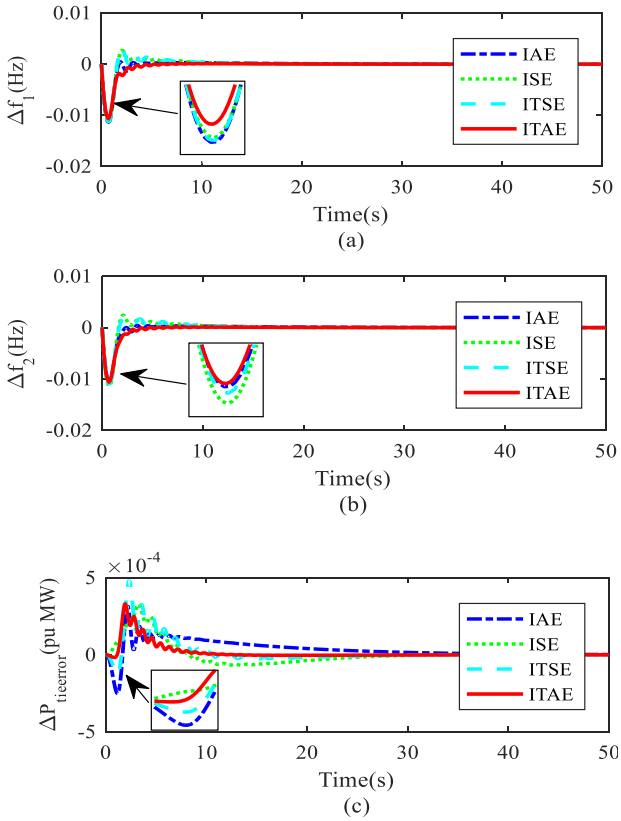

FIGURE 13. (a) Area-1 frequency deviation. (b) Area-2 frequency deviation. (c) Tie-line power deviation.

As the charges move in the search space, their position changes. Since charges represent the particle/population, the position of the particle changes and approaches the best-fit position. The velocity and position of the charge i in d dimension is given by the following expression:

$$\begin{aligned} V_i^d(t+1) &= rand()^* V_i^d(t) + a_i^d(t) \\ X_i^d(t+1) &= X_i^d(t) + V_i^d(t+1) \end{aligned} \tag{39}$$

where $rand()$ is a uniform random number in the interval [0,1] , $a_i^d(t)$ denotes the acceleration of an ith particle in dth dimension at any time t. The charge of the particle is evaluated by using a suitable charge function given by (42), assuming that the charge of each particle is equal.

$$Q_i(t) = Q_j(t) \quad i, j = 1, 2.....N \tag{40}$$

$$q_i(t) = \exp\left(\frac{fit_i(t) - worst(t)}{best(t) - worst(t)}\right) \tag{41}$$

$$Q_i(t) = \frac{q_i(t)}{\sum_{i=1}^{N} q_i(t)} \tag{42}$$

where fit_i is the fitness value of the ith particle at any time t.

AEFA adopts a learning strategy to improve its performance. $P_j^d(t)$ in (37) signifies the local best fitness history of jth particle and Q_i, Q_j represents the global best fitness history of the particles. By following all the strategies and laws, QO-AEFA eventually reaches the best-fit position.

A comparative analysis is carried out with various optimization techniques in the simulation results and discussions section.

Algorithm Quasi-Opposition-Based Artificial Electric Field Algorithm (QO-AEFA)

Bounds of the controller parameters serve as a constraint for the optimization process. Population size is assumed as 20 in the proposed algorithm and the number of iterations is taken 10. The different controller parameters with constraints that are manifested in the appendix are optimized with the proposed QO-AEFA algorithm. Whereas simulation runtime is considered as 50 seconds for the optimization process.

The algorithm for QO-AEFA is presented below:

Randomly initialize the population of solutions of size N as $(X_1(t), X_2(t).....X_N(t))$ in the search range $[X_{\min}, X_{\max}]$.

Initialize the velocity to a random value.

Set iteration $t = 0$

Reproduction and updating

while stopping criterion is not met do

Calculate the quasi opposite of the populations.

Evaluate the fitness value of the populations and their quasi opposite number.

Select the best N population

Calculate $K(t)$, $best(t)$ and $worst(t)$

Calculate the total force in each direction $F_i(t)$

Calculate the acceleration $a_i(t)$

$$V_i^d(t+1) = rand()^* V_i^d(t) + a_i^d(t)$$
$$X_i^d(t+1) = X_i^d(t) + V_i^d(t+1)$$

Check bounds of the variables

end while

VI. SIMULATION RESULTS AND DISCUSSION

Performance evaluation of the proposed controller and optimization technique is carried out by considering different cases of the test power system model. The analysis under different conditions is shown in the figure and tabular form. All the simulations and analysis are performed in MATLAB/SIMULINK® tool-box with variable step and ode45 solver. The different numerical parameters have been given in the Appendix section of the paper, and the MATLAB programming code of the QO-AEFA is written in (.m file). The simulation is run for 50 seconds and step load perturbation of 0.01 p.u is considered. GRC of 10 %per minute (i.e. 0.00167/second) and GDB ($N_{g1} = 0.8$, $N_{g2} = -0.2/P_i$) is considered for thermal system and GRC of 20% per minute (i.e. 0.00334/second) for biogas system in both areas. A different analysis is as follows:

A. SYSTEM DYNAMIC PERFORMANCE ANALYSIS

The proposed algorithm i.e., QO-AEFA, is chosen to optimize the controller gains parameters of an interconnected

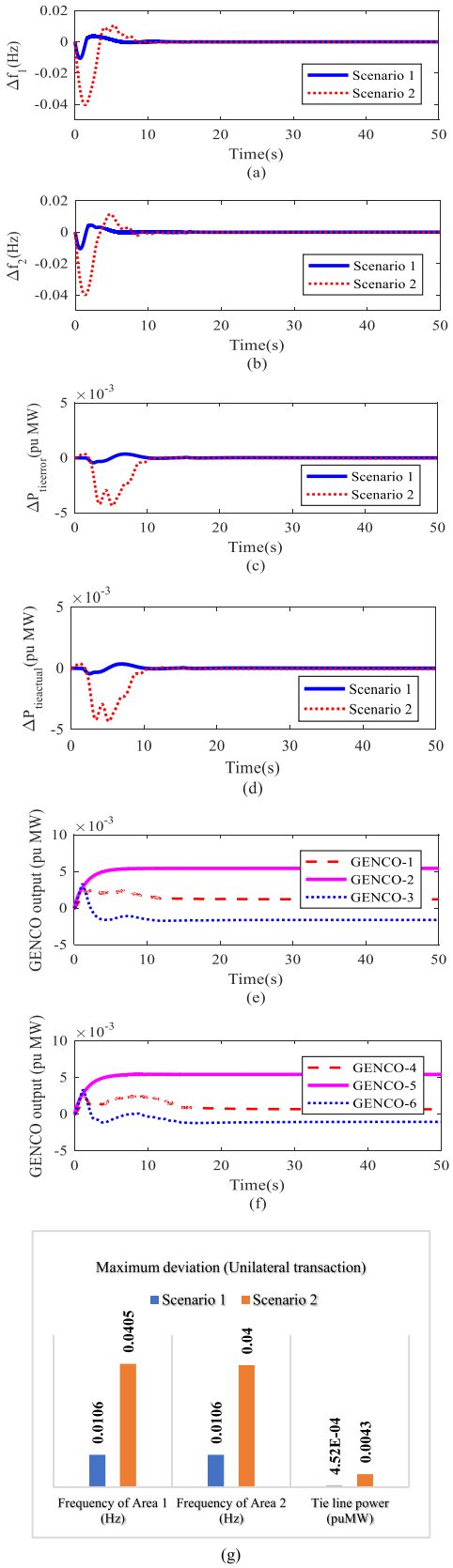

FIGURE 14. Unilateral transaction. (a) Area-1 frequency deviation. (b) Area-2 frequency deviation. (c) Tie-line error power deviation. (d) Tie-line actual power deviation. (e) Area-1 GENCO output for scenario-1. (f) Area-2 GENCO output for scenario-1. (g) Chart portraying improvement in scenario-1.

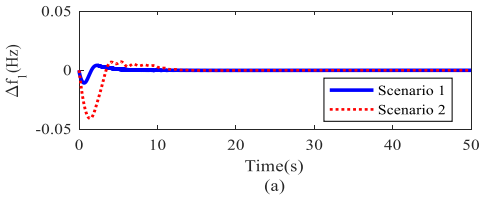

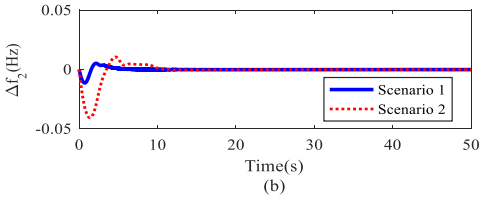

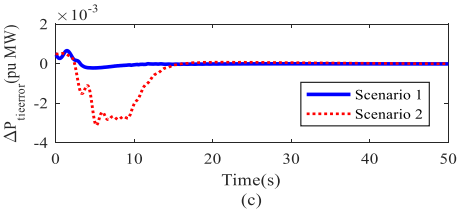

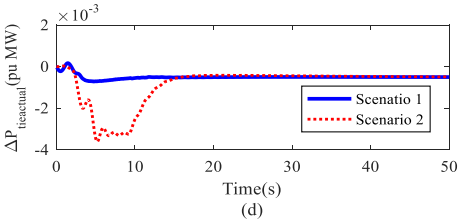

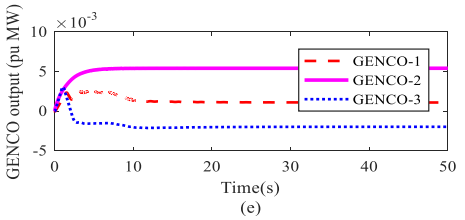

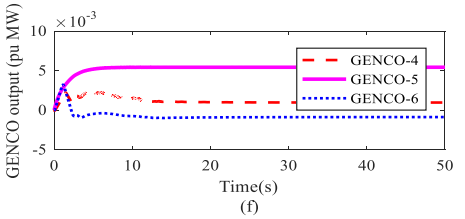

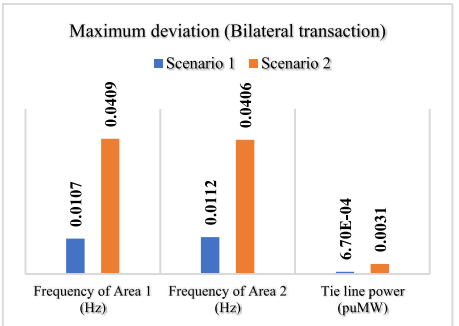

FIGURE 15. Bilateral transaction. (a) Area-1 frequency deviation. (b) Area-2 frequency deviation. (c) Tie-line power deviation. (d) Tie-line actual power deviation. (e) Area-1 GENCO output for scenario-1. (f) Area-2 GENCO output for scenario-1. (g) Chart portraying improvement in scenario-1.

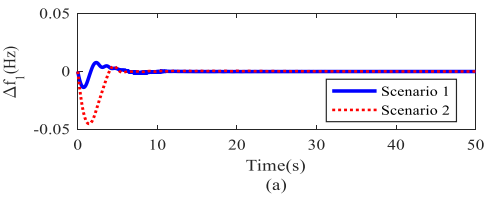

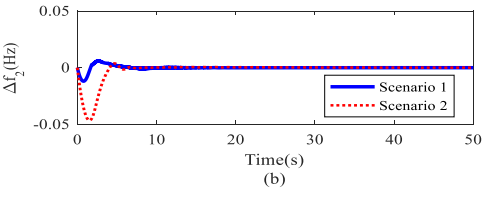

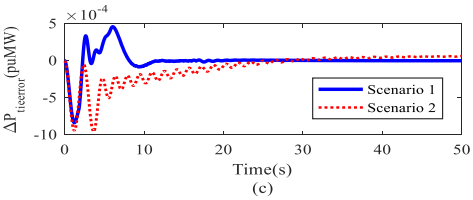

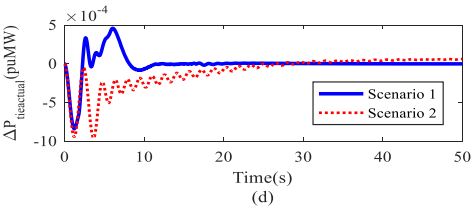

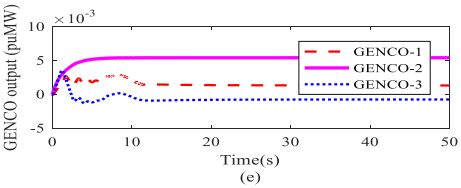

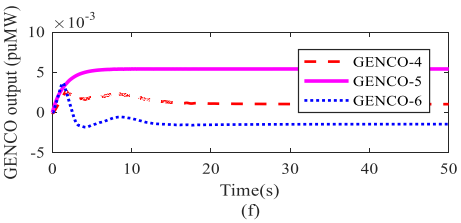

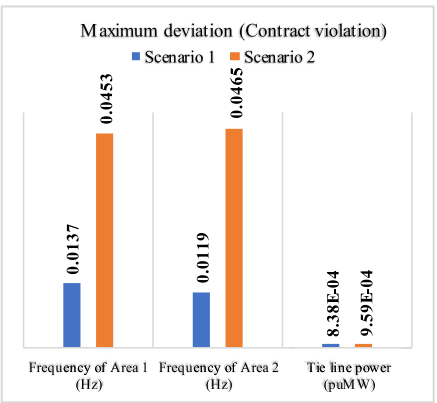

FIGURE 16. Contract violation. (a) Area-1 frequency deviation. (b) Area-2 frequency deviation. (c) Tie-line power deviation. (d) Tie-line actual power deviation. (e) Area-1 GENCO output for scenario-1. (f) Area-2 GENCO output for scenario-1. (g) Chart portraying improvement in scenario-1.

TABLE 4. Maximum deviation and settling time in deregulation case.

	Δf_1		Δf_2		ΔP_{tie_error}	
Unilateral transaction						
	M. D (Hz)	S. T (s)	M.D (Hz)	S. T (s)	M.D (puMW)	S. T (s)
S-1	0.0106	9.05	0.0106	15.28	4.52E-04	30.35
S-2	0.0405	8.31	0.04	10.61	0.0043	12.79
Bilateral transaction						
	Δf_1		Δf_2		ΔP_{tie_error}	
	M. D (Hz)	S. T (s)	M. D (Hz)	S. T (s)	M. D (puMW)	S. T (s)
S-1	0.0107	9.7675	0.0112	11.61	6.70E-04	17.80
S-2	0.0409	12.184	0.0406	10.51	0.0031	28.17
Contract violation						
	Δf_1		Δf_2		ΔP_{tie_error}	
	M. D (Hz)	S. T (s)	M. D (Hz)	S. T (s)	M. D (puMW)	S. T (s)
S-1	0.0137	10.28	0.0119	11.45 22	8.38E-04	17.54
S-2	0.0453	5.66	0.0465	6.14	9.59E-04	39.96

TABLE 5. Tuned parameter values for scenario-1 and scenario-2.

Controller gains	Unilateral transaction		Bilateral transaction		Contract violation	
	S-1	S-2	S-1	S-2	S-1	S-2
ω_{c_1}	1.20	0.68	1.04	0.50	1.37	2.00
ω_{c_2}	1.26	0.55	0.92	1.08	1.26	0.51
ω_{o_1}	7.19	3.78	9.03	5.85	6.82	2.02
ω_{o_2}	3.97	6.45	7.40	10.0 0	7.24	5.94
k_1	0.49	0.00	0.13	0.00	0.61	0.27
k_2	0.61	0.84	0.58	0.31	0.71	1.00
K_{P_1}	1.21	2.00	1.22	0.77	1.18	0.04
K_{I_1}	1.36	1.24	1.48	1.22	1.35	0.02
k_3	0.59	0.96	0.15	0.51	0.52	0.94
k_4	0.58	0.13	0.69	0.00	0.57	0.68
K_{P_2}	1.45	0.00	0.97	0.39	0.50	0.00
K_{I_2}	1.36	2.00	1.11	1.40	0.98	0.15
$K_{P_{11}}$	1.61	-	1.26	-	0.92	-
$K_{I_{11}}$	0.53	-	0.65	-	0.97	-
$K_{D_{11}}$	1.49	-	0.81	-	1.11	-
$K_{P_{22}}$	0.69	-	1.53	-	0.92	-
$K_{I_{22}}$	0.72	-	0.50	-	0.75	-
$K_{D_{22}}$	0.94	-	0.96	-	1.19	-
N_1	51.10	-	65.53	-	77.83	-
N_2	85.51	-	58.99	-	65.41	-

deregulated power system model. Each area consists of three GENCOs and two DISCOs, as portrayed in Fig. 1. System parameter values are reflected in the appendix. In this section, the three cases of deregulated system unilateral, bilateral,

TABLE 6. Frequency, Tie-line power deviation and settling time values for distinct controllers.

Controller	Δf_1		Δf_2		ΔP_{tie_error}	
	M. D (Hz)	S.T(s)	M D (Hz)	S T(s)	M D (puMW)	S.T(s)
I	0.0135	11.30	0.0135	11.67	4.9E-04	49.88
PI	0.0131	49.07	0.0130	49.02	2.4E-04	49.95
PID	0.0108	12.23	0.0108	12.29	4.2E-04	25.30
PIDN	0.0111	4.26	0.011	4.09	1.7E-04	32.62
Fuzzy-PI	0.0116	9.16	0.0111	8.79	0.0011	16.32
LADRC	0.0126	13.20	0.0126	13.35	7.8E-05	31.81
Proposed	**0.0106**	**4.99**	**0.0106**	**4.49**	**3.3E-04**	**10.78**

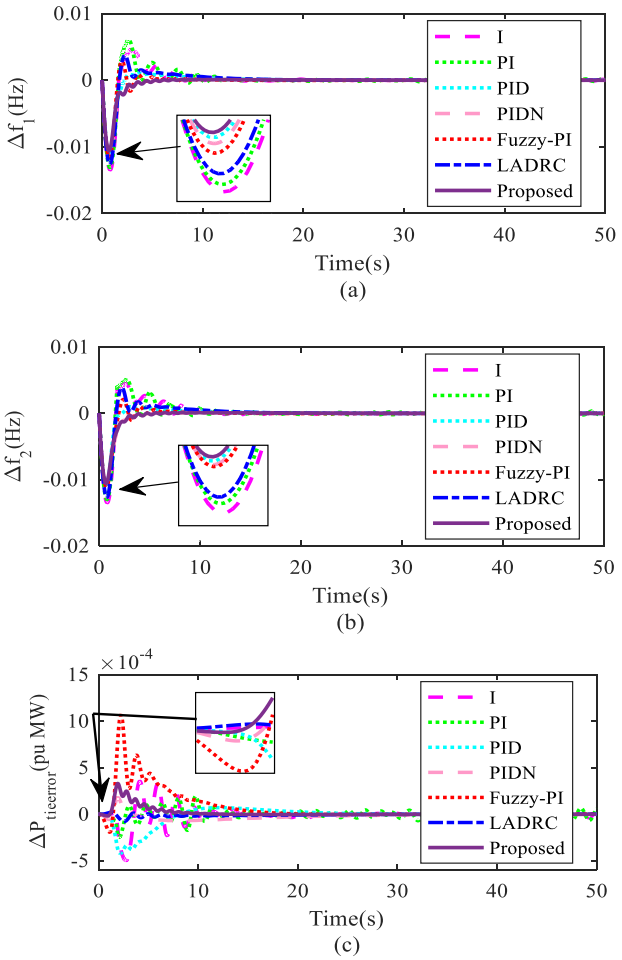

FIGURE 17. (a) Area-1 frequency deviation. (b) Area-2 frequency deviation. (c) Tie-line power deviation.

and contract violation are analyzed under two scenarios: scenario 1 with EV and scenario 2 without EV system. Simulation results can be visualized with appropriate figures and tables.

1) CASE-I UNILATERAL TRANSACTION

In this type of structure, the DISCOs can contract the power only from the GENCOs in their own areas. The DISCOs demand 0.005 p.u. load from GENCOs in their respective

TABLE 7. Tuned values of controller gains.

Controller gains	I	PI	PID	PIDN	Fuzzy-PI	LADRC	Proposed
ω_{c_1}	-	-	-	-	-	1.02	**0.98**
ω_{c_2}	-	-	-	-	-	1.10	**0.69**
ω_{o_1}	-	-	-	-	-	5.99	**5.58**
ω_{o_2}	-	-	-	-	-	5.52	**8.84**
b_{0_1}	-	-	-	-	-	6.22	-
b_{0_2}	-	-	-	-	-	6.79	-
k_1	-	-	-	-	0.60	-	**0.06**
k_2	-	-	-	-	0.53	-	**0.97**
K_{P_1}	-	0.65	0.97	0.80	0.74	-	**1.38**
K_{I_1}	1.38	1.28	0.55	0.18	1.03	-	**1.83**
K_{D_1}	-	-	1.53	1.17	-	-	-
k_3	-	-	-	-	0.46	-	**0.20**
k_4	-	-	-	-	0.77	-	**0.82**
K_{P_2}	-	1.16	1.42	1.01	1.42	-	**1.88**
K_{I_2}	1.12	1.52	1.44	0.40	0.35	-	**1.08**
K_{D_2}	-	-	1.63	1.80	-	-	-
N_1'	-	-	-	170.5	-	-	-
N_2'	-	-	-	116.5	-	-	-
$K_{P_{11}}$	1.35	0.72	0.35	1.17	1.03	1.09	**1.83**
$K_{I_{11}}$	0.57	0.93	0.31	0.91	0.18	0.98	**1.75**
$K_{D_{11}}$	1.93	1.67	1.47	1.17	0.45	1.18	**0.15**
$K_{P_{22}}$	0.94	0.96	1.54	1.29	1.192	0.79	**1.84**
$K_{I_{22}}$	0.632	0.53	0.417	1.291	0.89	0.69	**1.73**
$K_{D_{22}}$	1.24	1.044	1.86	0.765	0.94	1.28	**0.391**
N_1	42.99	35.73	43.80	82.54	60.63	56.8	**87.22**
N_2	54.69	85.53	42.73	69.35	65.86	55.78	**75.62**

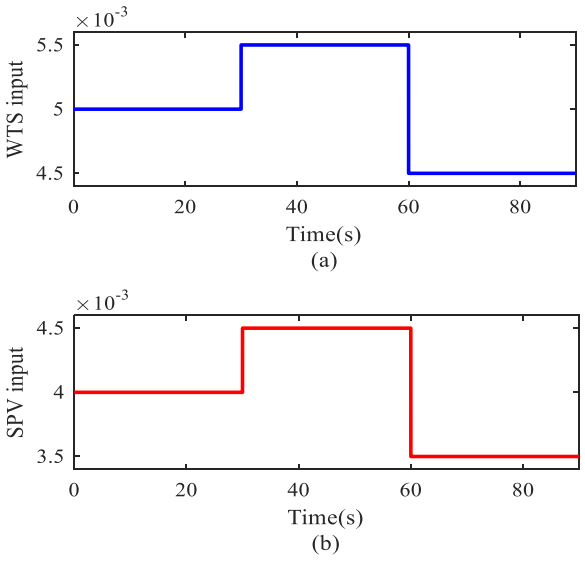

FIGURE 18. (a) Input to WTS. (b) Input to SPV.

areas. The local load demand for each area is:

$$\Delta P_D = 0.005 + 0.005 = 0.01\text{p.u.}$$

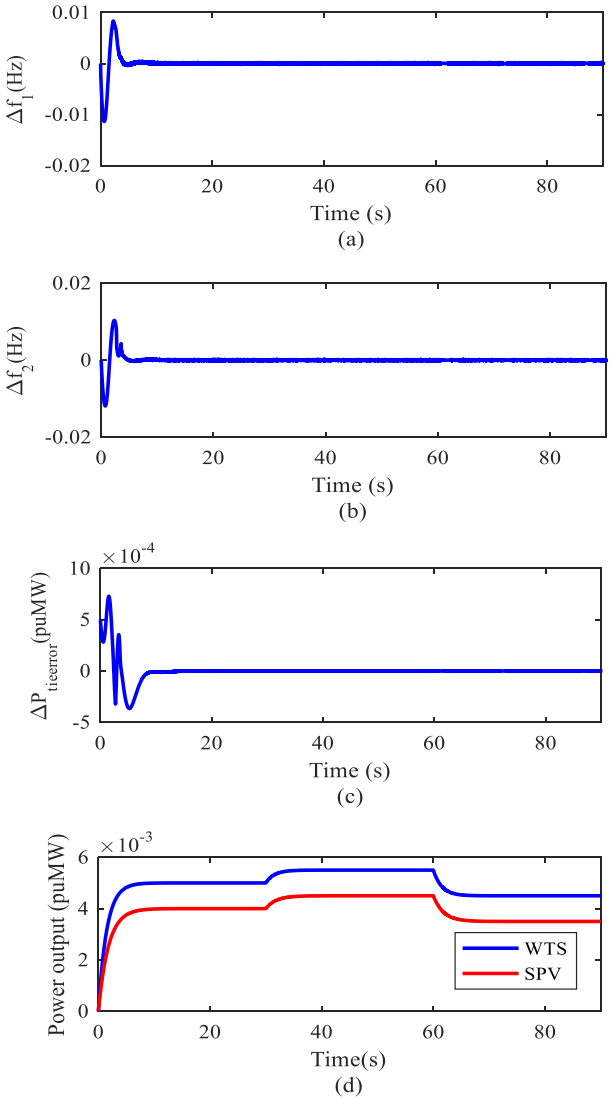

FIGURE 19. Random weather condition. (a) Area-1 frequency deviation. (b) Area-2 frequency deviation. (c) Tie-line power deviation. (d) Power output WTS and SPV.

TABLE 8. System performance for random weather condition.

Δf_1		Δf_2		ΔP_{tie_error}	
M. D (Hz)	S. T (s)	M. D (Hz)	S. T (s)	M. D (puMW)	S. T (s)
0.0114	6.9800	0.0119	6.9800	7.27E-04	8.9800

DPM is as follows:

$$DPM = \begin{bmatrix} 0.6 & 0.4 & 0 & 0 \\ 0.3 & 0.3 & 0 & 0 \\ 0.1 & 0.3 & 0 & 0 \\ 0 & 0 & 0.6 & 0.4 \\ 0 & 0 & 0.3 & 0.3 \\ 0 & 0 & 0.1 & 0.3 \end{bmatrix} \quad (43)$$

The system performance is shown in Fig. 14 (a to d) in both the scenarios with EV and without EV. The GENCOs output in the scenario: 1 is shown in Fig. 14 (e) and Fig. 14 (f).

TABLE 9. Tuned values of controller gains for random weather condition.

Controller gains	Tuned values
ω_{c_1}	1.1845
ω_{c_2}	0.9505
ω_{o_1}	3.2917
ω_{o_2}	3.7683
k_1	0.3977
k_2	0.5134
K_{P_1}	0.367
K_{I_1}	0.8459
k_3	0.119
k_4	0.1112
K_{P_2}	0.178
K_{I_2}	0.9125
$K_{P_{11}}$	1.192
$K_{I_{11}}$	1.2335
$K_{D_{11}}$	0.8574
$K_{P_{22}}$	1.7064
$K_{I_{22}}$	0.7637
$K_{D_{22}}$	0.1015
N_1	82.2739
N_2	77.4209

TABLE 10. Sensitivity analysis for 10% change in system parameters.

	Δf_1		Δf_2		ΔP_{tie_error}	
	M. D (Hz)	S. T (s)	M.D (Hz)	S. T (s)	M. D (puMW)	S. T (s)
Nominal	**0.0107**	**9.76**	**0.0112**	**11.61**	**6.7E-04**	**17.80**
			+10% change			
B	0.0106	8.70	0.0111	10.75	6.5E-04	16.38
T_g	0.0108	8.54	0.0113	12.01	6.6E-04	18.23
R_{th}	0.0107	11.34	0.0112	10.98	6.7E-04	19.20
T_r	0.0107	8.72	0.0112	12.09	6.7E-04	17.56
T_t	0.0107	8.69	0.0112	11.88	6.7E-04	18.57
			-10% change			
B	0.0108	11.43	0.0113	8.13	6.7E-04	14.35
T_g	0.0107	8.63	0.0112	10.36	6.7E-04	16.28
R_{th}	0.0107	8.57	0.0112	10.85	6.7E-04	17.66
T_r	0.0107	8.31	0.0112	8.38	6.7E-04	14.13
T_t	0.0107	10.48	0.0112	7.93	6.7E-04	16.88

We observed that EV improves system performance after the disturbance has occurred. Fig. 14 (g) represents the significance of the scenario: 1. The maximum deviation and settling time of the area frequency and tie-line power is realized in Table 4. Controller gains values tuned by QO-AEFA are given in Table 5 for scenario-1 and scenario-2.

2) CASE-II BILATERAL TRANSACTION

In this case, the DISCOs and GENCOs share the bilateral contract and submit the agreement to the ISO. Here each disco is demanding 0.005 p.u. power from the GENCOs, resulting

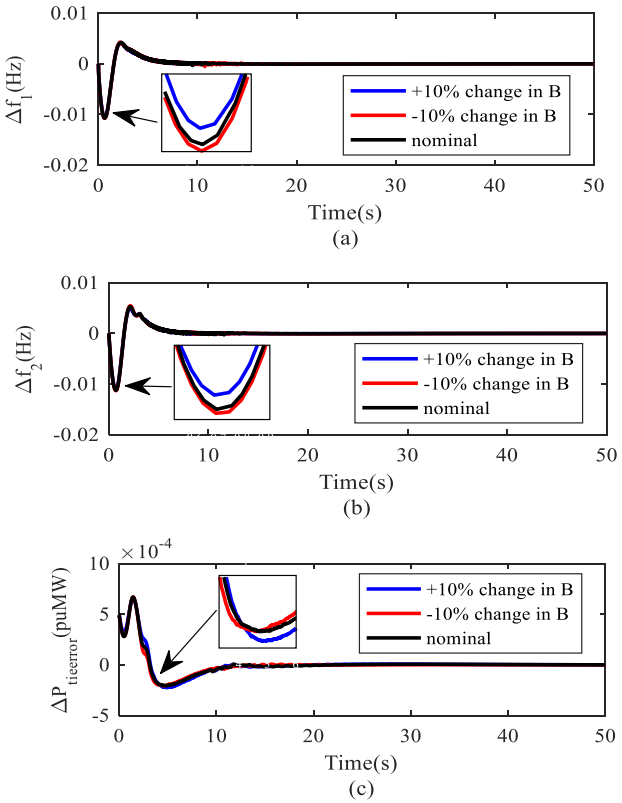

FIGURE 20. Variation in frequency bias constant. (a) Area-1 frequency deviation. (b) Area-2 frequency deviation. (c) Tie-line power deviation.

in total local load demand in each area as:

$$\Delta P_D = 0.005 + 0.005 = 0.01\text{p.u.}$$

DPM in this case is:

$$DPM = \begin{bmatrix} 0.2 & 0.3 & 0.3 & 0.2 \\ 0.15 & 0.2 & 0 & 0.15 \\ 0.15 & 0.1 & 0.15 & 0 \\ 0.2 & 0.25 & 0.2 & 0.35 \\ 0.15 & 0.15 & 0.2 & 0.2 \\ 0.15 & 0 & 0.15 & 0.1 \end{bmatrix} \quad (44)$$

Fig. 15 shows the system performance in 'with EV' and 'without EV' scenarios along with GENCO output in scenario:1. System performance values, tuned controller gains are visualized in Table 4 and Table 5.

3) CASE –III CONTRACT VIOLATION

This is simply a special case in the above two cases where the DISCOs violate the contract. In such a situation the uncontracted power is supplied by the GENCO of the same area in which DISCO violates the contract. Here pool-based transaction case is considered where DISCO 1 of area 1 violates the contract by demanding extra 0.001 p.u. power. Local load demand in area 1 modifies to:

$$\Delta P_D = (0.005 + 0.001) + 0.005 = 0.011\text{p.u.} \quad (45)$$

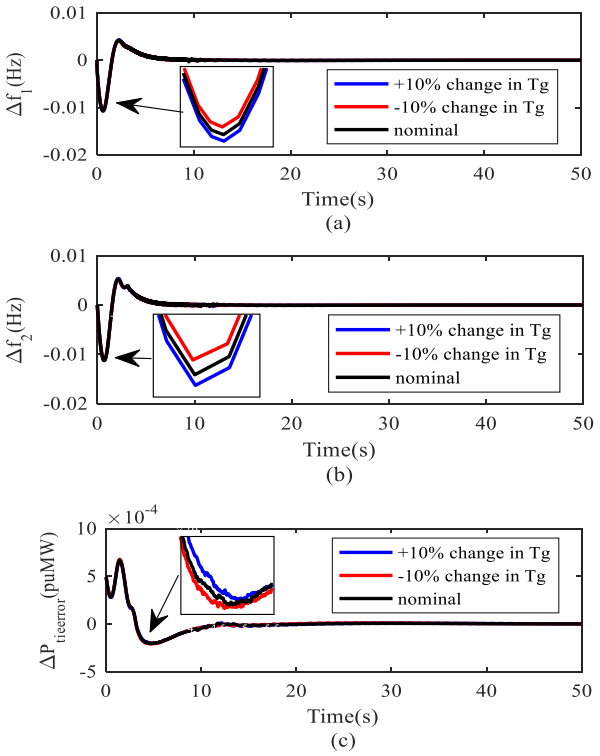

FIGURE 21. Variation in governor time constant. (a) Area-1 frequency deviation. (b) Area-2 frequency deviation. (c) Tie-line power deviation.

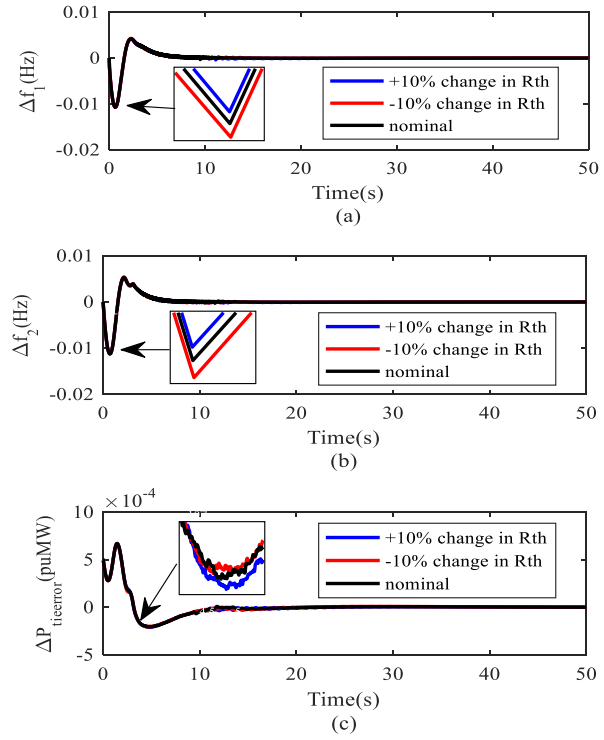

FIGURE 22. Variation in regulation constant of thermal power plant. (a) Area-1 frequency deviation. (b) Area-2 frequency deviation. (c) Tie-line power deviation.

System performance is shown in Fig. 16 where 'with EV' and 'without EV' scenario along with GENCO output in

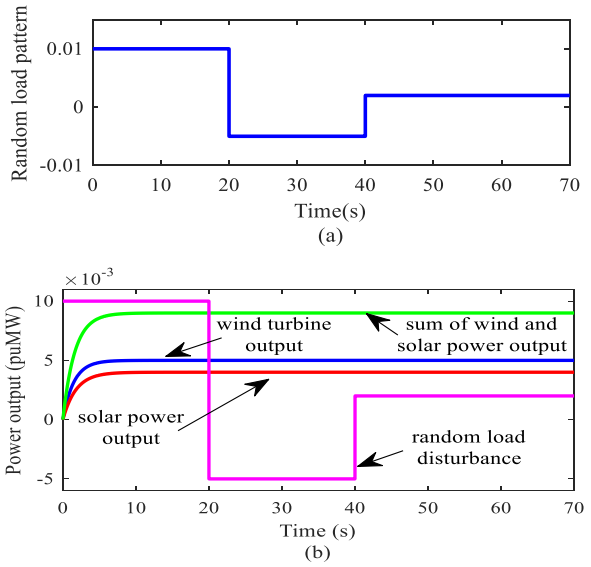

FIGURE 23. (a) Random load. (b) Power output of WTS and SPV.

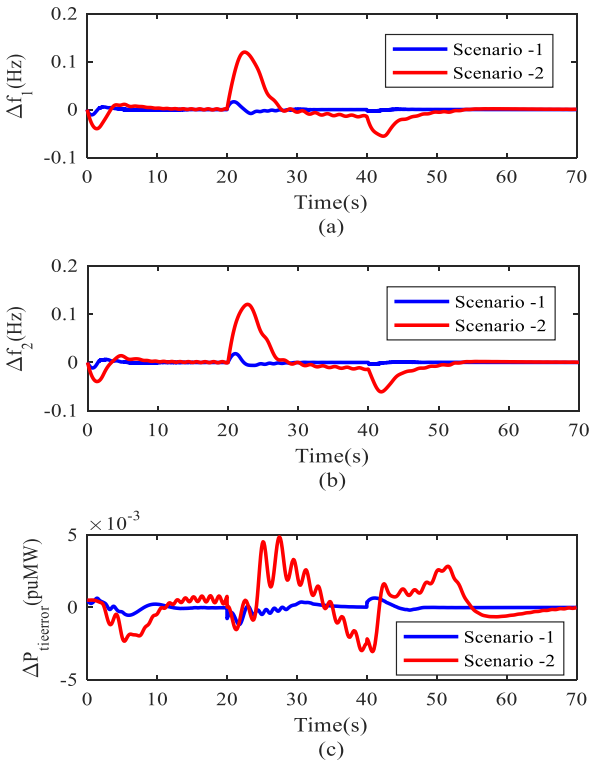

FIGURE 24. Random load condition. (a) Area-1 frequency deviation. (b) Area-2 frequency deviation. (c) Tie-line power deviation.

scenario: 1 is presented. Area frequency deviation, tie-line power deviation, and settling time are reported in Table 4 whereas tuned controller gains are shown in Table 5.

B. COMPARATIVE PERFORMANCE OF PROPOSED CONTROLLER WITH DISTINCT OTHER CONTROLLER

The superiority of the proposed controller is visualized by comparing its performance with other eminent controllers.

TABLE 11. Tuned parameter values for scenario-1 and scenario-2 for random load condition.

CONTROLLER GAINS	SCENARIO-1	SCENARIO-2
ω_{c_1}	1.369	1.4113
ω_{c_2}	1.2012	1.1181
ω_{o_1}	8.616	6.6426
ω_{o_2}	4.8302	6.1066
k_1	0.3564	0.1379
k_2	0.6404	0.4617
K_{P_1}	0.7541	0.6337
K_{I_1}	1.5984	0.5345
k_3	0.7281	0.4118
k_4	0.37	0.3353
K_{P_2}	1.1555	1.3302
K_{I_2}	1.749	1.2776
$K_{P_{11}}$	0.7623	-
$K_{I_{11}}$	1.1557	-
$K_{D_{11}}$	1.2703	-
$K_{P_{22}}$	0.9116	-
$K_{I_{22}}$	0.803	-
$K_{D_{22}}$	1.4192	-
N_1	82.3081	-
N_2	88.2228	-

TABLE 12. Maximum deviation and settling time for various optimization technique.

Optimization technique	Δf_1		Δf_2		ΔP_{tie_error}	
	M.D (Hz)	S. T (s)	M. D (Hz)	S. T (s)	M. D (puMW)	S. T (s)
PSO	0.0107	6.98	0.0107	6.98	4.2E-04	8.98
TLBO	0.0115	6.98	0.012	6.98	3.18E-04	8.98
Whale	0.0121	6.98	0.0121	6.98	4.18E-05	8.98
GWO	0.0108	6.98	0.0108	6.98	2.9E-05	8.98
AEFA	0.011	6.98	0.0116	6.98	1.1E-03	8.98
Proposed	**0.0106**	**4.99**	**0.0106**	**4.49**	**3.3E-04**	**10.78**

The controllers which are considered for comparison are I, PI, PID, PIDN, Fuzzy-PI, and LADRC. From the comparison Table 6 and Fig. 17, we can observe that the proposed controller outperforms the other controllers, giving less frequency deviation and settling time. Table 7 contains tuned values of the controller gains.

C. ANALYSIS UNDER RANDOM WEATHER CONDITION

The degree of effectiveness of the proposed controller is analyzed under random weather conditions in a bilateral case. In this reference, WTS and SPV are given uncertain random input as shown in Fig. 18 (a) and Fig. 18 (b). The corresponding system performances are shown in Fig. 19. Table 8 signifies that the proposed controller is effective under random weather conditions. We see that frequency

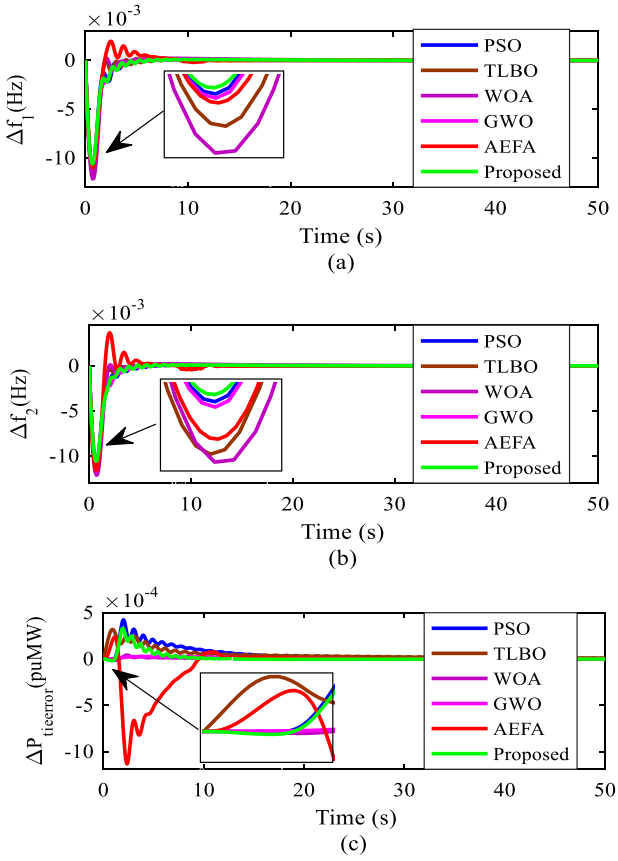

FIGURE 25. Optimization techniques. (a) Area-1 frequency deviation. (b) Area-2 frequency deviation. (c) Tie-line power deviation.

and tie-line excursion subsides, resulting in stable output. The proposed controller gain parameters optimized with the proposed QO-AEFA algorithm are provided in Table 9. Further analysis clearly reveals the dynamic performances under random weather conditions.

D. SENSITIVITY ANALYSIS

Sensitivity analysis is carried out to test the robustness of the controller under parameter variation due to uncertain reasons. It is desired that the controller performance should not deviate much following a slight change in system parameters. Following the system, parameters are varied by ±10% of the nominal value in both the areas: frequency bias constant (B), governor time constant (T_g), regulation constant of thermal power plant (R_{th}), reheat time constant (T_r), and turbine time constant (T_t).

This analysis is carried out in a bilateral case, and the profile of frequency aberration and tie-line power aberration pertaining to the sensitivity analysis is demonstrated. Fig. 20 to Fig. 22 portray the variation in B, T_g, and R_{th}, respectively, and they manifest that there is a minute deviation from system performance at nominal value. It is also supported by numerical data in Table 10 that the proposed controller optimized by QO-AEFA shows robust performance

TABLE 13. Controller gain values for different optimization technique.

Controller gains	PSO	TLBO	WOA	GWO	AEFA	Proposed
ω_{c_1}	0.6233	0.6641	0.5	0.5932	0.6092	**0.9802**
ω_{c_2}	0.6967	0.5	0.5	0.5221	0.8526	**0.6942**
ω_{o_1}	2.6195	10	10	7.03	7.7532	**5.5865**
ω_{o_2}	8.8715	10	10	7.262	9.3342	**8.8472**
k_1	0.3544	0	0.2615	0.1964	0.1547	**0.0671**
k_2	0.6635	1	0.6015	0.5893	0.9846	**0.9745**
K_{P_1}	1.9261	0.9841	0.2098	1.9019	1.1296	**1.3814**
K_{I_1}	1.2583	2	0.2667	0.9284	1.8232	**1.8374**
k_3	0.0547	0	0.3816	0.2544	0.6962	**0.2048**
k_4	0.9765	0.568	0.4473	0.7827	0.3844	**0.8262**
K_{P_2}	1.2647	0.2422	0.3333	1.4097	0.733	**1.8888**
K_{I_2}	0.7657	0.1901	0.1481	0.7365	1.5072	**1.0814**
$K_{P_{11}}$	0.858	2	0.0516	1.7151	1.741	**1.8314**
$K_{I_{11}}$	1.8966	0.0856	1.7989	1.383	1.0348	**1.7548**
$K_{D_{11}}$	0.9022	1.1808	0.4014	1.0839	1.361	**0.1591**
$K_{P_{22}}$	1.225	0	0.2822	1.2306	0.4766	**1.8401**
$K_{I_{22}}$	1.2599	2	2	1.5533	0.9041	**1.7348**
$K_{D_{22}}$	1.6574	2	0.3867	0.5065	0.7716	**0.391**
N_1	25	25	25	30.455	37.5149	**87.2271**
N_2	25	25	25	33.537	62.752	**75.6234**

TABLE 14. Comparison data for Case-1.

	Δf_1		Δf_2		ΔP_{tie_error}	
	M. D (Hz)	S. T (s)	M. D (Hz)	S. T (s)	M. D (puMW)	S. T (s)
KPS Parmar *et al.* [25]	0.1968	45	0.0716	48	0.025	46
Proposed controller	0.1761	15.68	0.0532	28.8	0.0201	36.72

as there is insignificant or no variation in system behavior following discrepancies in the system parameters. Hence it is assured that tuned controller gain values can be utilized without resetting it under a slight variation in system parameters.

E. ANALYSIS WITH RANDOM LOAD VARIATION

In the real system, the load on the system continuously changes throughout the day. Therefore, the controller should be capable of maintaining system frequency under randomly varying loading conditions. Controller performance is checked under random load conditions in both the scenarios mentioned above and is found to work well under this condition. The random load is applied as shown by Fig. 23 (a) and the associated solar and wind power output in the bilateral case is reported in Fig. 23 (b). The system performance is shown in Fig. 24. The tuned parameters of the controller gains are provided in Table 11.

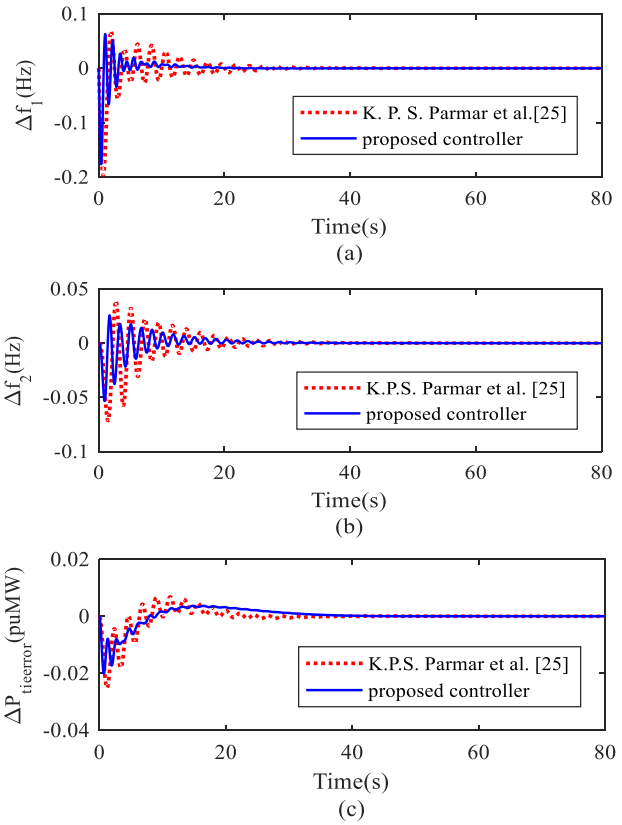

FIGURE 26. K.P.S. Parmar *et al.* [25]. (a) Area-1 frequency deviation. (b) Area-2 frequency deviation. (c) Tie-line power deviation. (d) Chart portraying improvement with proposed controller.

F. DYNAMIC SYSTEM PERFORMANCE WITH EMPLOYED OPTIMIZATION TECHNIQUE

Additionally, the efficacy of the proposed optimization technique is verified with the PSO, TLBO, WOA, GWO, and AEFA. The corresponding transient responses are manifested in Fig. 25 (a to c) that evidently depicts the supremacy of the proposed optimization technique over other algorithms in the literature. The maximum deviation and settling time of the employed optimization techniques are reflected in Table 12, and the tuned controller gain parameters are reported in Table 13 for the investigated test system.

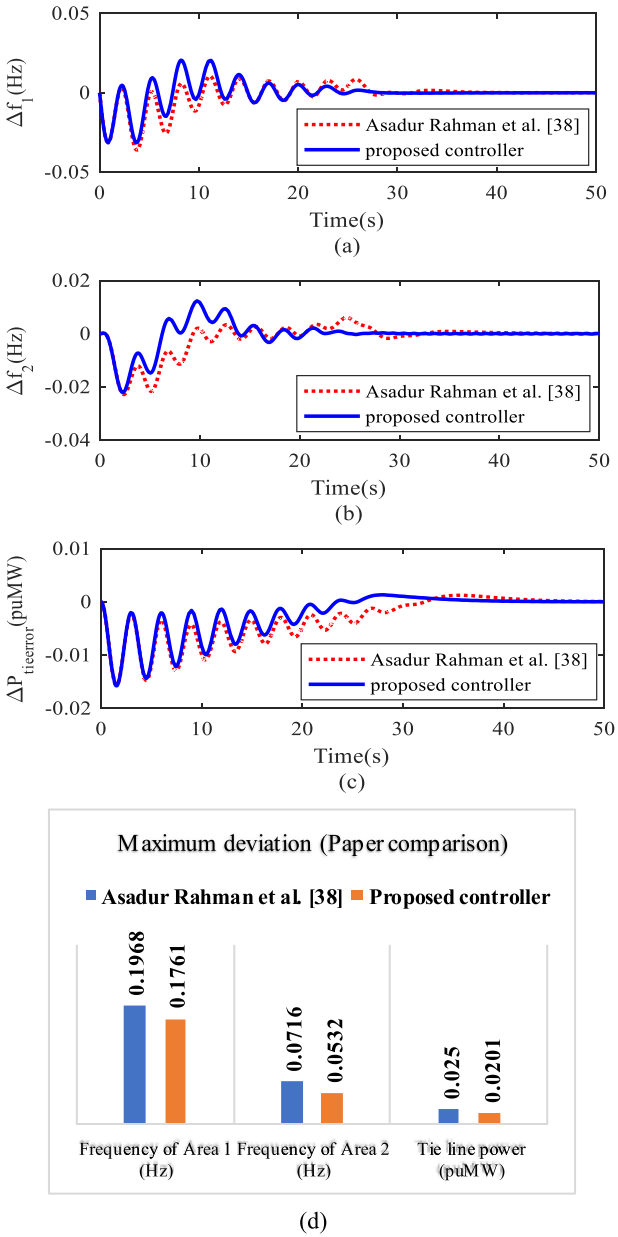

FIGURE 27. Asadur Rahman *et al.* [38]. (a) Area-1 frequency deviation. (b) Area-2 frequency deviation. (c) Tie-line power deviation. (d) Chart portraying improvement with proposed controller.

TABLE 15. Comparison data for Case-2.

	Δf_1		Δf_2		ΔP_{tie_error}	
	M. D (Hz)	S. T (s)	M. D (Hz)	S. T (s)	M. D (puMW)	S. T (s)
Asadur Rahman *et al.* [38]	0.0363	38.86	0.0229	42.82	0.0157	47.80
Proposed controller	0.0315	34.32	0.0221	24.14	0.0156	45.41

G. COMPARISON WITH PREVIOUS LITERATURE

The dynamic performance of the designed controller is counter compared with two pieces of literature: K.P.S. Parmar *et al.* [25] and Asadur Rahman *et al* [38] to check its effectiveness in their system. We found that the proposed controller shows improved performance. Fig. 26 and Fig. 27 portray the response of the system as compared to the literature. Table 14 and Table 15 contain the numerical values of the comparison whereas Table 16 gives the tuned controller gains of the proposed controller.

TABLE 16. Tuned parameter values for literature comparison.

Controller gains	with K.P.S. Parmar *et al.* [25]	with Asadur Rahman *et al.* [38]
ω_{c_1}	1.4263	1.3841
ω_{c_2}	1.4454	1.5718
ω_{o_1}	8.3978	6.6601
ω_{o_2}	7.654	3.7738
k_1	0.001	0.7835
k_2	0.8563	0.001
K_{P_1}	1.7858	0.001
K_{I_1}	0.5579	1.654
k_3	0.8891	0.7495
k_4	0.2008	0.6333
K_{P_2}	0.7524	0.6293
K_{I_2}	0.0106	1.6612

VII. CONCLUSION

The prolific demeanor of Automatic Generation Control with conventional sources as well as distributed generation has been examined and investigated for improved frequency regulation with different conditions and scenarios of deregulation. DG units are comprehensively investigated for random weather conditions and random load variations. For the realistic analysis of the AGC framework, non-linearities like GDB, GRC along with boiler dynamics are also considered and investigated. A novel and maiden application of the Fuzzy PI and LADRC controller is successfully proposed and implemented for the studied test system. Furthermore, EV's are addressed into the proposed AGC system to accomplish uncontracted demand that exhibits promising and encouraging results. Also, a novel QO-AEFA algorithm is proposed for acquiring the different optimal gain parameters of the intended employed controllers for the tested system. ITAE has been considered as an objective function for the suggested AGC paradigm. The performance adequacy of the proposed algorithm has also been validated over other employed algorithms in the literature. A comparative performance evaluation of the proposed controller with some other controllers is manifested to endorse its potency for the analyzed work. Consequently, the proposed controller substantially ameliorates the frequency and tie-line power excursions of the studied test system. Distinct improved results are presented to authenticate the endeavor for the system dynamic responses. The potency of the proposed AGC scheme and optimization technique is well verified and tested by considering distinct

cases under deregulation, comparative analysis with other controllers, sensitivity analysis followed by random load change, and comparison with works in previous literature. Subsequently, in the future, a demand response strategy may be employed in the proposed system to further ameliorate the frequency and tie-line power flow instability concern. Also, the proposed controller may be enhanced with some other novel knowledge-based controller. The proposed methodology incorporating FACT devices, possibly with the enhanced controller might be able to reflect the promising impact on the performance of the system. As a consequence of the challenges faced due to the exhaustion of fossil fuels, the integration of renewable and bio-renewable energy sources such as solar tower, hydrogen power, geothermal, bio-diesel, bio-ethanol, etc. in the studied test system along with solar and wind would be a potential alternative for years to come.

APPENDIX

Controller parameters with constraints: Controller bandwidth of Area 1 ($0 \leq \omega_{c_1} \leq 2$), controller bandwidth of Area 2 ($0 \leq \omega_{c_2} \leq 2$), observer bandwidth of Area 1 ($2 \leq \omega_{o_1} \leq 10$), observer bandwidth of Area 2 ($2 \leq \omega_{o_2} \leq 10$), scaling factor of Fuzzy controller in Area 1 ($0 \leq k_1 \leq 1$), scaling factor of Fuzzy controller in Area 1 ($0 \leq k_2 \leq 1$), proportional gain of Fuzzy-PI controller in Area 1 ($0 \leq k_{p_1} \leq 2$), proportional gain of Fuzzy-PI controller in Area 2 ($0 \leq k_{p_2} \leq 2$), scaling factor of Fuzzy controller in Area 2 ($0 \leq k_3 \leq 1$), scaling factor of Fuzzy controller in Area 2 ($0 \leq k_4 \leq 1$), integral gain of Fuzzy-PI controller in Area 1 ($0 \leq k_{I_1} \leq 2$), integral gain of Fuzzy-PI controller in Area 2 ($0 \leq k_{I_2} \leq 2$), proportional gain of PIDN controller in Area 1 ($0 \leq k_{P_{11}} \leq 2$), integral gain of PIDN controller in Area 1 ($0 \leq k_{I_{11}} \leq 2$), derivative gain of PIDN controller in Area 1 ($0 \leq k_{D_{11}} \leq 2$), proportional gain of PIDN controller in Area 2 ($0 \leq k_{P_{22}} \leq 2$), integral gain of PIDN controller in Area 2 ($0 \leq k_{I_{22}} \leq 2$), derivative gain of PIDN controller in Area 2 ($0 \leq k_{D_{22}} \leq 2$), filter constant of PIDN controller in Area 1 ($0 \leq N_1 \leq 100$), filter constant of PIDN controller in Area 2 ($0 \leq N_2 \leq 100$), Rated capacity of area-1 (P_{r1}) and area-2 (P_{r2}) = 2000MW. Thermal power plant: $T_g = 0.08$ s; $K_r = 0.5$; $T_r = 10$s; $T_t = 0.3$ s; $N_{g1} = 0.8$; $N_{g2} = 0.2/\pi$; GRC: 10% /minute. Boiler dynamics: $K_1 = 0.85$; $K_2 = 0.095$; $K_3 = 0.92$; $C_B = 200$; $T_D = 0$s; $T_F = 10$s; $K_{IB} = 0.030$; $T_{IB} = 26$ s; $T_{RB} = 69$ s. Biogas power plant: $X_g = 0.6$ s; $Y_g = 1.0$ s; $b_v = 0.05$ s; $T_F = 0.23$ s. $T_{CR} = 0.01$ s; $T_{CD} = 0.2$ s; GRC: 20% /minute. Regulation: $R_{th} = R_g = 2.4$ Hz/p.u. MW. Damping constant: B = 0.425 p.u. MW/Hz. system: $K_P = 120$; $T_P = 20$ s. Distributed generation: WTS: $K_{WTS} = 1$, $T_{WTS} = 1.5$ s, SLP = 0.005 p.u.; SPV: $K_{SPV} = 1$, $T_{SPV} = 1.8$ s, SLP = 0.004 p.u.; AE: $K_{AE} = 0.002$, $T_{AE} = 0.5$s; FC: $K_{FC} = 0.01$, $T_{FC} = 4$s; DEG: $K_{DEG} = 1$, $T_{DEG} = 2$s; BESS: $K_{BESS} = -0.003$, $T_{BESS} = 0.1$s; FESS: $K_{FESS} = -0.01$, $T_{FESS} = 0.1$s.Tie-line: Rated capacity of tie-line = 200MW; Loading = 50%; $a_{12} = P_{r1}/P_{r2} = 1$; $T_{12} = 0.0866$. Nominal frequency: f = 60Hz; Nominal inertia constant: H = 5s. M. D and S. T represent maximum deviation and settling time. S-1 and S-2 reflect scenario-1 and scenario-2.

REFERENCES

[1] O. Elgerd and C. Fosha, "Optimum megawatt-frequency control of multi-area electric energy systems," *IEEE Trans. Power App. Syst.*, vol. PAS-89, no. 4, pp. 556–563, Apr. 1970.
[2] M. Ma, C. Zhang, X. Liu, and H. Chen, "Distributed model predictive load frequency control of the multi-area power system after deregulation," *IEEE Trans. Ind. Electron.*, vol. 64, no. 6, pp. 5129–5139, Jun. 2017.
[3] M. Deepak and R. J. Abraham, "Load following in a deregulated power system with Thyristor controlled series compensator," *Int. J. Electr. Power Energy Syst.*, vol. 65, pp. 136–145, Feb. 2015.
[4] H. Bevrani and T. Hiyama, *Intelligent Automatic Generation Control*. Boca Raton, FL, USA: CRC Press, 2011.
[5] P. Kumar and D. P. Kothari, "Recent philosophies of automatic generation control strategies in power systems," *IEEE Trans. Power Syst.*, vol. 20, no. 1, pp. 346–357, Feb. 2005.
[6] L. L. Lai, *Power System Restructuring and Deregulation: Trading Performance and Information Technology*. New York, NY, USA: Wiley, 2001, pp. 258–284.
[7] P. K. Hota and B. Mohanty, "Automatic generation control of multi source power generation under deregulated environment," *Int. J. Electr. Power Energy Syst.*, vol. 75, pp. 205–214, Feb. 2016.
[8] A. Dutta and S. Debbarma, "Frequency regulation in deregulated market using vehicle-to-grid services in residential distribution network," *IEEE Syst. J.*, vol. 12, no. 3, pp. 2812–2820, Sep. 2018.
[9] P. Sharma, A. Prakash, R. Shankar, and S. K. Parida, "A novel hybrid salp swarm differential evolution algorithm based 2DOF tilted-integral-derivative controller for restructured AGC," *Electr. Power Compon. Syst.*, vol. 47, nos. 19–20, pp. 1775–1790, Mar. 2020.
[10] J. Mudi, C. K. Shiva, and V. Mukherjee, "Multi-verse optimization algorithm for LFC of power system with imposed nonlinearities using three-degree-of-freedom PID controller," *Iranian J. Sci. Technol., Trans. Electr. Eng.*, vol. 43, no. 4, pp. 837–856, May 2019.
[11] R. K. Sahu, S. Panda, and G. T. C. Sekhar, "A novel hybrid PSO-PS optimized fuzzy PI controller for AGC in multi area interconnected power systems," *Int. J. Electr. Power Energy Syst.*, vol. 64, pp. 880–893, Jan. 2015.
[12] S. Kayalvizhi and D. M. V. Kumar, "Load frequency control of an isolated micro grid using fuzzy adaptive model predictive control," *IEEE Access*, vol. 5, pp. 16241–16251, 2017.
[13] A. H. G. Haroun and Y.-Y. Li, "A novel optimized hybrid fuzzy logic intelligent PID controller for an interconnected multi-area power system with physical constraints and boiler dynamics," *ISA Trans.*, vol. 71, pp. 364–379, Nov. 2017.
[14] A. Annamraju and S. Nandiraju, "Robust frequency control in a renewable penetrated power system: An adaptive fractional order-fuzzy approach," *Protection Control Modern Power Syst.*, vol. 4, no. 1, p. 16, Aug. 2019.
[15] Y. Arya, "A new optimized fuzzy FOPI-FOPD controller for automatic generation control of electric power systems," *J. Franklin Inst.*, vol. 356, no. 11, pp. 5611–5629, Jul. 2019.
[16] S. Prasad, S. Purwar, and N. Kishor, "Load frequency regulation using observer based non-linear sliding mode control," *Int. J. Electr. Power Energy Syst.*, vol. 104, pp. 178–193, Jan. 2019.
[17] S. Saxena and Y. V. Hote, "Stabilization of perturbed system via IMC: An application to load frequency control," *Control Eng. Pract.*, vol. 64, pp. 61–73, Jul. 2017.
[18] K. Liu, J. He, Z. Luo, X. Shen, X. Liu, and T. Lu, "Secondary frequency control of isolated microgrid based on LADRC," *IEEE Access*, vol. 7, pp. 53454–53462, 2019.
[19] C. Bhavanisankar and K. R. Sudha, "An adaptive technique to control the load frequency of hybrid distributed generation systems," *Soft Comput.*, vol. 23, no. 23, pp. 12385–12400, Mar. 2019.
[20] A. Saha and L. C. Saikia, "Combined application of redox flow battery and DC link in restructured AGC system in the presence of WTS and DSTS in distributed generation unit," *IET Gener., Transmiss. Distrib.*, vol. 12, no. 9, pp. 2072–2085, May 2018.
[21] M.-H. Khooban, T. Dragicevic, F. Blaabjerg, and M. Delimar, "Shipboard microgrids: A novel approach to load frequency control," *IEEE Trans. Sustain. Energy*, vol. 9, no. 2, pp. 843–852, Apr. 2018.

[22] S. Debbarma and A. Dutta, "Utilizing electric vehicles for LFC in restructured power systems using fractional order controller," *IEEE Trans. Smart Grid*, vol. 8, no. 6, pp. 2554–2564, Nov. 2017.
[23] M.-H. Khooban, T. Niknam, M. Shasadeghi, T. Dragicevic, and F. Blaabjerg, "Load frequency control in microgrids based on a stochastic noninteger controller," *IEEE Trans. Sustain. Energy*, vol. 9, no. 2, pp. 853–861, Apr. 2018.
[24] Y. Arya, "Effect of electric vehicles on load frequency control in interconnected thermal and hydrothermal power systems utilising CF-FOIDF controller," *IET Gener., Transmiss. Distrib.*, vol. 14, no. 14, pp. 2666–2675, Jul. 2020.
[25] K. P. S. Parmar, S. Majhi, and D. P. Kothari, "LFC of an interconnected power system with multi-source power generation in deregulated power environment," *Int. J. Electr. Power Energy Syst.*, vol. 57, pp. 277–286, May 2014.
[26] V. Donde, M. A. Pai, and I. A. Hiskens, "Simulation and optimization in an AGC system after deregulation," *IEEE Trans. Power Syst.*, vol. 16, no. 3, pp. 481–489, Aug. 2001.
[27] J. Kumar, K.-H. Ng, and G. Sheble, "AGC simulator for price-based operation. II. Case study results," *IEEE Trans. Power Syst.*, vol. 12, no. 2, pp. 533–538, May 1997.
[28] S. Izadkhast, P. Garcia-Gonzalez, P. Frias, L. Ramirez-Elizondo, and P. Bauer, "An aggregate model of plug-in electric vehicles including distribution network characteristics for primary frequency control," *IEEE Trans. Power Syst.*, vol. 31, no. 4, pp. 2987–2998, Jul. 2016.
[29] X. Li, Y.-J. Song, and S.-B. Han, "Frequency control in micro-grid power system combined with electrolyzer system and fuzzy PI controller," *J. Power Sour.*, vol. 180, no. 1, pp. 468–475, May 2008.
[30] Y. Arya, "Improvement in automatic generation control of two-area electric power systems via a new fuzzy aided optimal PIDN-FOI controller," *ISA Trans.*, vol. 80, pp. 475–490, Sep. 2018.
[31] Z. Gao, "Active disturbance rejection control: A paradigm shift in feedback control system design," in *Proc. Amer. Control Conf.*, 2006, pp. 2399–2405.
[32] D. Wang, D. Tan, and L. Liu, "Particle swarm optimization algorithm: An overview," *Soft Comput.*, vol. 22, no. 2, pp. 387–408, Jan. 2018.
[33] R. V. Rao, V. J. Savsani, and D. P. Vakharia, "Teaching–learning-based optimization: A novel method for constrained mechanical design optimization problems," *Comput.-Aided Des.*, vol. 43, no. 3, pp. 303–315, Mar. 2011.
[34] S. Mirjalili, S. M. Mirjalili, and A. Lewis, "Grey wolf optimizer," *Adv. Eng. Softw.*, vol. 69, pp. 46–61, Mar. 2014.
[35] S. Mirjalili and A. Lewis, "The whale optimization algorithm," *Adv. Eng. Softw.*, vol. 95, pp. 51–67, May 2016.
[36] A. Yadav, "AEFA: Artificial electric field algorithm for global optimization," *Swarm Evol. Comput.*, vol. 48, pp. 93–108, Aug. 2019.
[37] S. Mahdavi, S. Rahnamayan, and K. Deb, "Opposition based learning: A literature review," *Swarm Evol. Comput.*, vol. 39, pp. 1–23, Apr. 2018.
[38] A. Rahman, L. C. Saikia, and N. Sinha, "Automatic generation control of an interconnected two-area hybrid thermal system considering dish-stirling solar thermal and wind turbine system," *Renew. Energy*, vol. 105, pp. 41–54, May 2017.

PRATEEK SHARMA received the bachelor's degree in electrical engineering from the Birsa Institute of Technology, Sindri, in 2010. He is currently pursuing the Ph.D. degree with NIT Patna, as a part-time scholar. He is currently an employed with Power Grid Corporation of India Limited as a Manager and posted at Gaya, Bihar. He has more than seven years of working experience in the field of operation and maintenance of EHVAC sub-stations. His current research interests include automatic generation control in multi-area power system and the impact of various controllers for restructured AGC.

ABHISHEK MISHRA received the B.Tech. degree in electrical engineering from REC Ambedkar Nagar, India, in 2016, and the M.Tech. degree in power system engineering from the National Institute of Technology, Patna, India, in 2020. His research interest includes load frequency control.

ABHISHEK SAXENA (Graduate Student Member, IEEE) received the bachelor's and master's degrees in electrical engineering from RGPV Bhopal (State Technical University of Madhya Pradesh), India, in 2012 and 2016, respectively. He is currently pursuing the Ph.D. degree from the National Institute of Technology, Patna, India. His current research interest includes demand response application in power systems for improved frequency regulation and renewable energy integration.

RAVI SHANKAR received the Ph.D. degree from the Indian Institute of Technology (Indian School of Mines) Dhanbad, India, in 2015. He is currently working as an Assistant Professor with the Department of Electrical Engineering, National Institute of Technology Patna, India. He has about seven years of teaching and research experience in different institutes across India. Prior to joining NIT Patna, he served as an Assistant Professor with KIIT University, Bhubaneswar, Odisha, and the National Institute of Technology (NIT) Mizoram, India. He has 48 research publications, which include journal of international repute, and international and national conferences. Seven Ph.D. research scholars are currently working under his guidance for their doctoral degrees in different areas of the power system. His major research interests include power system restructuring, soft computing application in power systems, artificial intelligent control design, FACTS device, renewable power, and energy storage application in power systems.